UNIVERSITY OF CALIFORNIA
RIVERSIDE

Earthquake Nucleation on Geometrically Complex Faults

A Dissertation submitted in partial satisfaction
of the requirements for the degree of

Doctor of Philosophy

in

Mechanical Engineering

by

Zijun Fang

December 2009

Dissertation Committee:
Dr. Guanshui Xu, Chairperson
Dr. James H. Dieterich
Dr. David D. Oglesby
Dr. Javier E. Garay

The Dissertation of Zijun Fang is approved:

_____

_____

_____

_____
Committee Chairperson

University of California, Riverside

ACKNOWLEDGEMENTS

This work would not have been possible without the help and support over the years of the following professors, colleagues, friends and family.

First, I express my sincere gratitude to both of my advisers, Dr. Guanshui Xu and Dr. James Dieterich. They have guided me in developing my research in the general subject of earthquake nucleation and showed me what characters that a good scientist should possess. I owe both of them more than words can express in developing myself as an independent researcher.

I also wish to thank Dr. David Oglesby. When I first start my Ph.D studies, I learned a lot of background knowledge of earthquakes from him. He helped me a lot in preparing my first journal articles from his valuable suggestions and efforts in revising the context. I would also thank him for his willingness to serve on the committee.

I am grateful to my fellow student, Gang Liu for meaningful discussions about numerical methods and mathematics. I also wish to thank my research colleague Keith Richards-Dinger for the insightful discussion about derivations of the generalized simple patch solution listed in the thesis.

Last but not the least, I would like to thank to my family and my girlfriend Qingyu Sun, for their support and trust.

ABSTRACT OF THE DISSERTATION

Earthquake Nucleation on Geometrically Complex Faults

by

Zijun Fang

Doctor of Philosophy, Graduate Program in Mechanical Engineering
University of California, Riverside, December 2009
Dr. Guanshui Xu, Chairperson

We have employed numerical approaches to study earthquake nucleation on geometrically complex faults governed by either slip-dependent friction or rate- and state- dependent friction. The interactions of fault friction, complex fault geometry and remote slow stressing from plate tectonics are investigated. In particular, we focus on characterizing three important physical aspects of an earthquake: the occurrence time, hypocenter location and earthquake source dimensions. Using a slip dependent friction law, we have investigated earthquake nucleation on both thrust and normal dip-slip faults with changes in dip (bends) at depth. Our results show that earthquakes tend to nucleate at shallower depth on thrust faults as compared to those on normal faults with the same geometry. Nucleation time increases significantly as the fault plane are bent more severe for both thrust and normal faults. Using the rate- and state-dependent friction, we studied nucleation on two parallel planar faults with step-over features. We focus on investigating how nucleation is affected by the offset between the two faults. We found that for faults with compressional step-overs, earthquakes tend to nucleate the end of the

overlapping zone when the offset is small, but generally nucleate further away from the overlapping end as the offset becomes larger. For faults with extensional step-overs, nucleation always occurs near the overlapping end for all the offsets considered. Our studies provide better understanding of the effects of fault geometry on earthquake nucleation and form a basis for the study of nucleation on large scale geometrically complex fault systems such as fault systems in Southern California. Our results may also provide realistic earthquake source conditions for rupture dynamics studies which at present largely employ ad hoc source conditions.

Table of Contents

List of Figures

Chapter 1

General Introduction

1.1 Frictional Constitutive Relations

Earthquakes are one of the most frightening and destructive phenomena in nature. In its most general sense, the term 'earthquake' is employed to describe any event that generates seismic waves. They are caused mostly by rupture of geological faults, but also by volcanic activity, landslides, mine blasts, and nuclear tests. In this paper, the term 'earthquake' only refers to tectonic earthquakes that happen on pre-existing faults. Extensive research on earthquake mechanisms has indicated that tectonic earthquakes result from unstable slip on faults due to a stick-slip frictional instability.

Two types of frictional constitutive models have been widely employed for fault instability analysis. One is the slip dependent friction, which assumes that the frictional resistance along fault interface is only a function of fault slip. Fault strength degrades from a peak resistance (static friction) down to a fixed residual frictional level (dynamic friction) sustained at large slip. Once slip stops after earthquake, fault strength regains its static value. With continuing remote stressing, slip can occur again when shear stress on the fault reaches the static friction threshold. Such friction laws were first introduced by *Ida* [1972] and *Palmer and Rice* [1973] by analogy to cohesive zone models of tensile fracture. The generic slip dependent friction characteristics have been widely observed

from laboratory experiments [e.g. *Ohnaka et al.*, 1987; *Ohnaka and Yamashita,* 1989]. In its most simplified case, friction is assumed to be linearly dependent on fault slip in which the friction coefficient μ is given as

$$\mu = \begin{cases} \mu_s - (\mu_s - \mu_d)\delta / d_c & \delta < d_c \\ \mu_d & \delta \geq d_c \end{cases} \tag{1-1}$$

where μ_s and μ_d are coefficients of static and dynamic friction respectively, and d_c is the critical slip-weakening distance [e.g., *Ida*, 1972; *Andrews*, 1976a; *Day*, 1982, *Madariaga et al.*, 1998]. This type of frictional constitutive relation has been widely used to model one-time quasi-static inter-seismic fault motion [e.g. *Shibazaki*, 2002; Zhang *et al*., 2004, 2006] and dynamic co-seismic fault motion [e.g. *Andrews*, 1976a, 1976b; *Okubo*, 1989; *Harris et al.*, 1991; *Harris and Day*, 1993, 1997; *Oglesby et al.*, 1998, *Duan and Oglesby*, 2005; *Dunham et al.*, 2003]. However, since such laws assume that slip stops and fault strength recovers to static value instantaneously, they do not model gradual strengthening after an earthquake.

The other general type of friction law is the rate- and state- dependent frictional model, which assumes that the friction is a function of slip rate and a fault state variable. Rate- and state- dependent friction is the 'state-of-the-art' understanding of macroscopic frictional properties, which has been widely documented for slip rates in the range of 10^{-9} ~ 10^{-3}m/s under a variety of experimental conditions and rock types [*Dieterich*, 1979, 1981; *Ruina*, 1983; *Blanpied and Tullis*, 1986; *Tullis and Weeks*, 1986; *Tullis*, 1988; *Linker and Dieterich*, 1992; *Beeler et al*., 1994; *Marone*, 1998; *Fry and Marone*, 2002].

The basic features of the rate- and state- dependent frictional behavior are well elaborated from the velocity jump tests. In a velocity jump test, sliding velocity is first held constant for a predetermined displacement and then abruptly changed to a new value. Figure 1.1 schematically shows how frictional resistance evolves in response to an instantaneous change of slip velocity. When sliding velocity is constant, the frictional resistance settles down to a constant 'steady state' value. Afterwards, with imposition of the sudden jump in velocity, friction instantaneously jumps with the same sign as the change of velocity. This instantaneous response is generally referred as the 'direct effect' that friction increases with increasing velocity. Following the instantaneous response, frictional resistance progressively evolves to a new 'steady state' value for the new sliding velocity over a certain amount of slip which is referred as the characteristic distance D_c. The evolution effect is of opposite sign to the change of slip velocity, which means that if the new sliding velocity is larger than the original velocity, the evolution effect will lead to a decrease of fault frictional resistance.

There is no full physical explanation for all of the observed rate- and state-dependent friction phenomena as seen from the velocity jump tests. However, recent studies have shed light on the physics for both the direct and evolution effects. In particular, the 'direct effect' is plausibly attributed to a thermally activated Arrhenius process at stressed asperity contacts [*Stesky*, 1977; *Heslot*, *et al*., 1994; *Chester*, 1994; *Brechet and Estrin*, 1994; *Baumberger*, 1997; *Berthoud and Baumberger*, 1999; *Lapusta et al.*, 2000; *Rice et al.*, 2001]. The 'evolution effect' is believed to be related to contact junction creep and a consequent increase in real contact area [*Wang and Scholz*, 1994;

Dieterich and Kilgore, 1996; *Baumberger and Berthoud*, 1999]. In this sense, the characteristic distance D_c can be interpreted as the slip required to renew the population of contacts and the state variable that used to quantify the evolution effect is equivalent to the lifetime of fault asperity contacts.

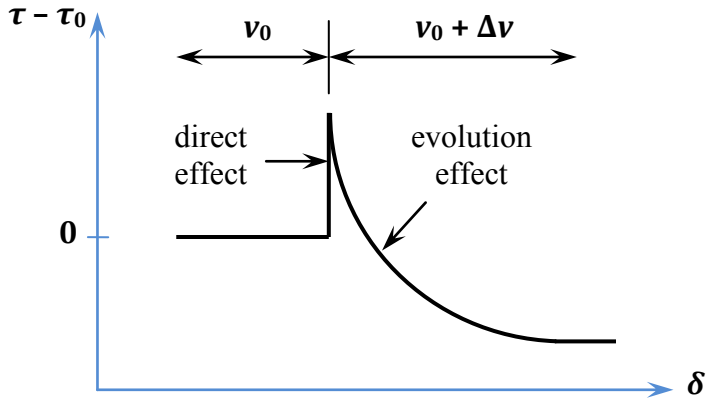

Figure 1-1. A schematic illustration of frictional response for a velocity jump experiment at fixed normal stress. The fault is first assumed to slide at a constant sliding velocity $v = v_0$, frictional resistance has a constant value τ_0. The slip rate jump causes an instantaneous increase in τ (direct effect), which then evolves to the new steady state value over a characteristic distance D_c.

A widely accepted mathematical representation of the rate- and state- dependent law is written as [*Dieterich*, 1979, 1981; *Ruina*, 1983]

$$\mu = \mu_0 + a \ln \frac{v}{v^*} + b \ln \frac{\theta v^*}{D_C} \tag{1-2}$$

where μ_0 is the friction coefficient at the reference slip rate v^*. θ is the state variable and D_c is the characteristic sliding distance. a and b are parameters which are positive and on the order of 10^{-2} [*Linker and Dieterich*, 1992; *Kilgore et al.*, 1993; *Blanpied et al.*, 1998a].

The evolution of the state variable, which empirically represents the evolution of contact populations between the sliding fault interfaces, is only found to be dependent on time and slip rate when normal stress is held constant. Mathematically, the evolution process can be fully described by the 'aging law' and written as

$$\frac{d\theta}{dt} = 1 - \frac{\theta v}{D_c} \tag{1-3}$$

The first term '1' on the right hand side represents laboratory experiment observations that a fault strengthens or 'heals' with time during stationary contact [*Dieterich*, 1972; *Beeler et al*., 1994; *Dieterich and Kilgore*, 1994; *Marone*, 1998]. The '$\theta v/D_c$' term represents the weakening rate due to slip. Because this term plays an important role in this dissertation, we define $\Omega \equiv \theta v/D_c$. Then, when $\Omega = 1$, sliding is at steady state ($d\theta/dt = 0$), i.e., the state variable remains constant. In response to a change of slip rate, the state variable θ will evolve to a new steady state over the characteristic distance D_c. When $\Omega < 1$, sliding is below steady state ($d\theta/dt > 0$). the state variable increases and healing takes the dominant role. When $\Omega > 1$, sliding is above steady state ($d\theta/dt < 0$). The state variable decreases, and weakening is dominant.

At steady state $\Omega = 1$, we have $\theta \equiv D_c/v$ and equation (1-2) reduces to

$$\mu_{ss} = \mu_0 + (a-b)\ln(v/v^*) \tag{1-4}$$

For $(a - b) < 0$, the interface weakens with increasing steady state slip rate and prone to instability while for $(a - b) > 0$, the interface is slip rate strengthening and always stable.

The parameter $(a - b)$ is a material property which is temperature dependent. For granite, it is negative at low temperature and become positive above 350°C [*Blanpied et al*., 1991, 1995, 1998b]. Since temperature increases with depth, then $(a - b)$ is depth dependent in nature. *Peacock and Wang* [1999] calculated a depth profile of parameters a and $(a - b)$ using temperature-dependent experimental data from a thermal structure model of southwest Japan subduction zone and found that $(a-b)$ is positive for depth greater than 25km.

In nature, faults are not simply frictional contact of bare rock surfaces. They are usually lined with wear detritus, called fault gouge. Shearing of these granular materials involves dilatancy, which will increase the parameter $(a - b)$ [*Scholz*, 1998]. Even for low temperatures near earth's surface, $(a - b)$ becomes positive since fault gouge is poorly consolidated. As depth increases, fault gouge consolidates and lithified due to elevated pressure and temperature. The effect of dilatancy to $(a - b)$ becomes negligible and $(a - b)$ is primarily controlled by temperature. Based on above discussion, earthquakes are not prone to occur in shallow depth at which fault gouge is poorly consolidated or in great depth at which temperature gets high enough to make $(a - b)$ positive. Generally, for

crustal faults, the upper transition depth from unstable to stable is about 4km and the lower transition occurs around 20km while for subduction zones the corresponding values are 10km and 45km respectively. In between is the seismogenic zone in which earthquakes are prone to occur. Laboratory studies with granitic rocks at temperatures and normal stresses appropriate for the seismogenic zone give values for a/b from around 0.7 to 0.9 for bare surfaces and for wet or nominally dry gouges Within this range, the presence of a layer of comminuted rock separating the sliding surfaces and increasing temperature favor larger a/b [*Biegel et al*., 1989; *Kilgore et al*., 1993; *Beeler et al*., 1996; *Blanpied et al*., 1998; *Marone*, 1998], while the presence of water favors lower a/b [*Dieterich and Conrad*, 1984; *Frye and Marone*, 2002].

A complication to the evolution of frictional state arises from the fluctuations of normal stress that generally prevail on natural faults. Fault slip will cause normal stress changes whenever the fault geometry is non-planar or the fault consists of non-homogeneous materials. Normal stress variation can also arise from regional stressing by plate tectonics and fault systems interactions. Normal stress variations alter sliding frictional resistance by direct coupling with shear stress as $\mu = \tau/\sigma$. Furthermore, it is also found that the evolution of the state variable θ also depends on normal stress σ [*Linker and Dieterich*, 1992]. To account for this effect, equation (1-3) becomes

$$\frac{d\theta}{dt} = 1 - \frac{\theta v}{D_c} - \frac{\alpha\theta\dot{\sigma}}{b\sigma} \tag{1-5}$$

where α is a constant which is found to be positive and with measured values in the range of $0.25 \leq \alpha \leq 0.5$. σ and $\dot{\sigma}$ stand for normal stress and its time derivative respectively. For convenience, the third term in the right hand side is denoted as $\Omega_n = \alpha\theta\dot{\sigma}/b\sigma$, which represents weakening or healing of a fault from normal stress variations. Considering the parameters in the term Ω_n, α is in the range of 0.25 ~ 0.5, b is on the order of 10^{-2}, σ is on the order of 10^8Pa and $\dot{\sigma}$, the changing rate of normal stress, is on the order of 10^{-3}Pa/s if normal stress variations are only results from remote plate stressing. Then Ω_n is on the order of $10^{-10}\theta$, suggesting that it becomes comparable to the healing term '1' when θ is on the order of 10^{10}s. Since θ can be interpreted as the contact lifetime of asperity contacts, the effect of normal stress variations on the evolution of the state variable becomes non-negligible when the fault has been locked for a long period comparable to several hundred years.

The rate- and state- dependent friction implies fault strengthening following earthquake rupture. Therefore, it is capable of describing various fault slip behaviors in a complete earthquake cycle. Fault models with rate- and state- dependent friction have generated various fault slip phenomena observed in nature such as episodic creep events or slow earthquakes [*Shibazaki* and *Iio*, 2003; *Liu and Rice*, 2005, 2007], earthquake dynamic slip [*Lapusta et al*, 2000; *Lapusta and Rice*, 2003], decelerating post-seismic creep [*Tse and Rice*, 1986; *Stuart*, 1988; *Kato and Hirasawa*, 1997; *Lapusta et al.*, 2000; *Lapusta and Rice*, 2003], and localized accelerating slip during earthquake nucleation [*Dieterich*, 1992; *Lapusta and Rice*, 2003; *Rubin and Ampuero*, 2005; *Ampuero and Rubin*, 2008; *Fang et al.*, 2009a].

In summary, rate- and state- dependent constitutive laws describes characteristic dependencies of friction on slip, slip rate, slip history, and normal stress history observed in laboratory studies, and it provides a unified framework for predictive modeling of the various fault sliding phenomena observed for faults in nature and in the laboratory. Therefore, most of the studies presented in this thesis employ rate- and state- dependent friction instead of the simple slip dependent friction.

1.2 Earthquake Nucleation on Planar Strike Slip Faults

Laboratory studies of micro-earthquakes between bare rock surfaces and simulated gouges have shown that earthquake rupture always initiates from a small area with localized unstable fault slip and then rapidly propagates over a much larger fault area [*Dieterich*, 1978, 1987; *Okubo and Dieterich*, 1984; *Ohnaka and Kuwahara*, 1990; *Ohnaka*, 1996; *Ohnaka and Shen*, 1999]. The events and interactions of fault slip that lead to the initiation of unstable slip are collectively defined as earthquake nucleation [*Dieterich*, 1987, 1992]. Models of earthquake nucleation process not only gives the evolution of fault sliding conditions and development of unstable slip but also reveals three important physical aspects of an earthquake at the initiation of earthquake rupture: earthquake occurrence time, hypocenter (epicenter) location and the dimension of the zone where earthquake rupture initiates. Characterization of nucleation process is of considerable interest in understanding a variety of earthquake phenomena. These include space-time patterns of seismicity such as foreshocks and aftershocks, triggering effects by tidal stresses and seismic waves, earthquake interactions, and scaling of premonitory

processes. In addition, by establishing initial conditions at the earthquake source, nucleation processes may also influence earthquake rupture dynamics. For example, nucleation zone dimension and the strength of the initiation process may affect the extent of earthquake rupture – an earthquake rupture may on average die out more quickly if it originates on a small weakly nucleating source compared to a large strongly nucleating source. Because the importance of nucleation process for understanding earthquakes, over last three decades, many theoretical and numerical studies on earthquake nucleation process have been done on simplified fault models with planar fault plane and under pure shear stressing conditions (constant normal stress).

Studies employed slip-dependent friction laws suggested that crustal earthquakes are resulted from unstable quasi-static fast creep. The hypocenter locations are controlled by fault friction properties, nearby elastic stress induced by fault slip and external stressing. *Stuart* [1979] and *Stuart and Mavko* [1979] analyzed development of unstable fault slip based on a postulated slip weakening relation between slip and shear strength with strain softening occurs beyond a peak stress. Those studies suggested that fault slip accelerates unstably at the place where the fault zone weakens with strain faster than the nearby elastic stress can decrease, and the accelerating precursory fault slip around the hypocenter may produce observable deformation changes at the free surface in the vicinity of the epicenter. *Li and Rice* [1983] analyzed how initially quasi-static upward progression of a zone of slip from the depth, along a transform plate margin, culminates in a great earthquake. Their results predict a final period of self-driven creep toward instability. The precursory surface straining in the self-driven stage is shown to proceed

at a distinctively higher slip rate over a time period between 3 ~ 10 months before the major earthquake. *Stuart et al.* [1985] modeled earthquake nucleation on Parkfiled faults using measurements of fault slip and ground deformation as constraints for model parameters. Accelerating creep around the hypocenter appears in all models examined by *Stuart* and the surface creep rate changes begin about 2 years before the coming earthquake, which are overall in good agreement with field data. *Shibazaki* [2002] investigated earthquake nucleation in a model with a depth-dependent slip dependent friction law that include a boundary between seismic-aseismic slip, the results suggested that earthquakes tend to nucleate at the boundary of seismic-aseismic transition at the bottom of the seismogenic zone. *Uenishi and Rice* [2003] considered nucleation process on a slip-weakening fault subjected to a heterogeneous, locally peaked 'loading' stressing. Slip initiates when the peak of the loading stress first reaches the stress level for start slip weakening after which slipping region grows until a critical nucleation length is reached. The nucleation length is proved to be independent of the shape of the loading stress distribution. Its universal value is proportional to elastic modulus and inversely proportional to slip-weakening rate.

Studies employed rate- and state- dependent friction also have shown that earthquake rupture is initiated from highly localized unstable fault slip. The hypocenter locations, occurrence times and nucleation zone dimensions are shown to be controlled by rate- and state- frictional properties, fault initial sliding conditions and remote tectonic loading. Based on rate- and state- friction constitutive relation, *Tse and Rice* [1986] interpreted the depth cutoff of crustal earthquake activities in terms of variations of

frictional properties with depth, from velocity weakening to velocity strengthening. Their simulation results on a two dimensional strike slip fault model with depth variation of frictional properties and temperature have shown features such as confinement of crustal earthquakes at shallow depth, the development of locked patch, the occurrence time of seismic cycles, the seismic stress drop and fault slip are generally in agreement with the observed characteristics of large scale strike-slip earthquakes.

By assuming conditions along fault are represented by the center-point values, *Dieterich* [1992] derived a simple patch solution which describes fault slip and the frictional state as explicit functions of time during nucleation process. By assuming a critical slip rate at which nucleation ends, the occurrence time can be explicitly solved from known initial and loading conditions. The solution forms the basis of a general formulation for rate of earthquake production resulting from an applied stressing history, which generates aftershocks following the Omori's decay law [*Dieterich*, 1994]. In addition, *Dieterich* [1992] also obtained analytical solutions for nucleation zone dimensions as $L = \eta G D_c / \xi \sigma$, where G is shear modulus and σ is normal stress. η is a factor that depends on the geometry of the fault patch and assumptions related to slip or stress conditions on the patch. ξ is a parameter related to the frictional constitutive laws and equals b critically. Because natural faults may have different geometry and stress conditions, η may vary for different faults but generally, *Dieterich* [1992] proposed that nucleation size should scales with a critical length

$$L_b = G D_c / b\sigma \tag{1-6}$$

Setting parameters with the typical values used in earthquake simulations as G = 40GPa, b = 0.01 and σ = 100MPa, $L_b = 40{,}000D_c$. Although the possible values of D_c for natural faults are still unknown, laboratory studies on meter size rocks reported D_c ranges from 10^{-6}m to 10^{-4}m [*Okubo and Dieterich*, 1984; *Dieterich and Kilgore*, 1996] which suggests that nucleation size should be on the order of meters. The occurrence of micro-earthquakes with source dimensions of a few meters demonstrate that nucleation zones on natural faults frequently have lengths of a few meters or less. Then, a fast creeping nucleation zone with area on the order of tens of square meters at the seismogenic depth about 10km below the Earth's surface is hardly to be detected by surface or even deep borehole seismometers.

Rice [1993] analyzed the effect of the minimum cell size of fault discretization on spatial and temporal distribution of fault slip. In order to give a valid solution from a discrete numerical model, the cell size h has to be smaller than the critical length h^*, which is denote by $L_{b\text{-}a}$ here

$$L_{b-a} = GD_c/(b-a)\sigma \tag{1-7}$$

which is the theoretical minimum nucleation size inferred from the critical stiffness of a single-degree-freedom system. *Lapusta and Rice* [2002] studied nucleation on 2D rate- and state- fault under a locally peaked stress and stressing rate. Their results showed that nucleation size does not match the simple estimates of nucleation zone size as L_b and $L_{b\text{-}a}$.

Rubin and Ampuero [2005] considered the subject of nucleation size in greater detail by exploring analytical quasi-static solutions of a rate and state dependent fault embedded in a two dimensional. For the 'aging' version of the evolution law for the state variable as shown by equation (1-3), they found two primary regimes for nucleation. The first operates well above steady state ($\Omega >> 1$) in which nucleation zone takes the form of a patch of fixed length which is proportional to b^{-1}, and has a minimum nucleation length $1.3774GD_c/b\sigma$. The second regime operates slightly above steady state ($\Omega \sim 1$) and initial localization is followed by a quasi-static nucleation zone expansion that the nucleation patch grows asymptotically proportional to $b/(b-a)^2$. Furthermore, they found nucleation always favor the fixed length scaling when $a/b < 0.3781$. However, for $a/b > 0.5$, together with the initial conditions used by *Rubin and Ampuero* [2005], nucleation zone always takes the appearance of an expanding crack with its half length approaching the maximum nucleation size

$$L_\infty = \frac{1}{\pi}\frac{b^2}{(b-a)^2}\frac{GD_c}{b\sigma} = \frac{1}{\pi}\frac{1}{(1-a/b)^2}L_b \tag{1-8}$$

which is derived from conservation of fracture energy. They further suggested that fault with a/b approaching 1 may have nucleation zone with its size much larger than L_b, for example, when $a/b = 0.98$, nucleation size is about $796L_b$. Extremely large fast creeping nucleation zone may generate signals detectable by surface seismometers as early warnings of imminent earthquakes.

The subject of nucleation zone dimension was further explored by *Fang et al.* [2009a]. Consistent with the result of *Rubin and Ampuero* [2005], they found that nucleation zone dimensions are controlled by both the value of Ω in the stage of fast accelerating slip and the frictional parameter a/b. From laboratory experiments, a/b is likely to be in the range of 0.7 ~ 0.9, which favors expansion during nucleation. However, Ω of the nucleating patch is controlled by initial conditions (initial slip rate, state variable and stress). Based on results from more than 1,000 simulations starting from different initial conditions, they found that large nucleation zones with significant expansion only occur for a very narrow range of sliding conditions. In addition, this critical range of conditions is not likely to be accessed by nucleation process starting from conditions right after a previous earthquake. It is also shown that external processes such as stress steps resulted from nearby earthquakes are also not likely to result in significant nucleation zone expansion. Thus, they suggested that nucleation zone size should generally comparable to L_b and extremely large nucleation zone may not appear in natural nucleation processes.

1.3 Earthquake Nucleation on Geometrically Complex Faults

Previous nucleation studies mostly employed fault models with planar fault plane under pure shear loading [*Tse and Rice*, 1986; *Dieterich*, 1992; *Rice*, 1993; *Lapusta and Rice*, 2002; *Rubin and Ampuero*, 2005; *Fang et al.*, 2009a]. However, natural faults are usually non-planar, having bends (Figure 2a), branches (2b) and stepover (2c) features [*Wesnousky*, 1988; *Zachariasen* and *Sieh*, 1995; *Zoback et al*, 1999; *Zampier et al*, 2003;

Brankman and *Aydin*, 2004]. Slip on faults with non-planar geometry induces normal stress variations. In addition, remote stressing tensor generally will not be perfectly aligned with every segment of a non-planar fault to exert pure shear loading. As a result, certain portions of a non-planar fault must be clamped or unclamped by remote loading.

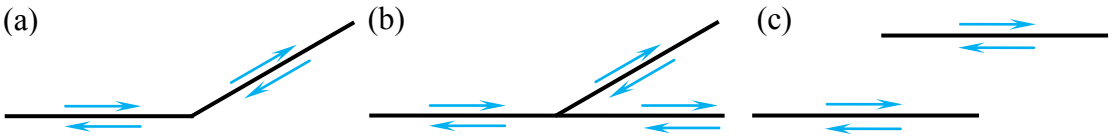

Figure 1-2: Schematic illustration of common geometric features on non-planar faults. (a) bend, (b) branch, (c) stepover.

Normal stress variations on non-planar faults resulting from fault slip and remote stressing will contribute to the nucleation process from two mechanisms. First, normal stress directly couples with shear stress in determining of friction coefficient μ. Second, from the expanded version of 'aging law' equation (1-5), the frictional state variable θ is affected by changes of normal stress, which alters friction coefficient. Therefore, it is reasonable to suspect that nucleation processes on non-planar faults may evolve quite differently as compared to those on idealized planar faults. In particular, evolution of fault sliding conditions may be altered by normal stress variations. Consequently earthquake occurrence times, nucleation size and nucleation location may be changed compared to cases with planar fault plane.

However, only a few studies have focus on the role of fault geometry in nucleation process. *Nielsen and Knopoff* [1998] modeled quasi-static rupture on a non-planar strike slip fault with bends. They concluded that extensional bends were preferred locations for earthquake nucleation, as expected from the reduced normal stress at these locations. Using a 2D quasi-static model with slip-dependent friction, *Zhang et al.*, [2004] systematically studied the effect of non-vertical dip-slip fault geometry on earthquake nucleation. The non-vertical dipping geometry results in a non-trivial vertical component of fault slip, which induces normal stress variations. Their results indicated that the coupling between slip, shear stress, and normal stress due to the fault's asymmetric geometry has a large effect on earthquake nucleation. In particular, for normal and thrust faults with the same geometric configuration, earthquakes tend to nucleate closer to the free surface for thrust faults. In the meanwhile, nucleation processes take less time to reach instability on thrust faults as well. *Zhang et al.*, [2006] further incorporated depth dependent frictional properties into their earlier dip-slip models. Their result showed that although depth dependent friction moves nucleation location further down-dip away from the free surface and reduces occurrence times, the basic effect of asymmetric dipping on nucleation process still holds: earthquakes nucleate farther up dip in a shorter time on thrust faults than those on normal faults as well. Their study suggested that fault geometry has equivalent (or even larger) importance for earthquake nucleation as depth dependent frictional heterogeneities which have been widely studied [*Stuart and Mavko*, 1979; *Stuart et al.*, 1985; *Tse and Rice*, 1986; *Rice*, 1993; *Stuart and Tullis*, 1995; *Shabazaki*, 2002].

Non-planar fault geometry is also known to have a large effect on earthquake rupture dynamics and distributions of co-seismic slip. Bends, stepovers and branches can have a strong effect on rupture propagation and fault slip which could results in stress buildups and reductions near such features that may affect nucleation of the next earthquake [*Bouchon and Streiff*, 1997; *Magistrale and Day,* 1999; *Harris et al.*, 2002; *Oglesby et al.*, 2003a, 2003b; *Duan and Oglesby*, 2005, 2008; *Oglesby*, 2005, 2007]. However, nucleation in turn can affect the next earthquake rupture. Rupture propagation and strong ground motion will be strongly affect by the hypocenter location and may be affected by nucleation zone size. Currently, most studies of earthquake rupture dynamics employed ad hoc nucleation information to generate earthquake ruptures [e.g. *Harris et al.*, 2002], which increases uncertainties in inferring realistic rupture behaviors based on their results. Therefore, it is also necessary to carry out more nucleation studies to give more realistic constraints for rupture dynamics studies, especially for those cases involving complex fault geometry, which makes guessing of possible nucleation location almost impossible because of all of the complexity.

This dissertation is dedicated to demonstrate the effect of complex fault geometry on earthquake nucleation. It is divided into four chapters. Chapter 1 gives a general introduction for frictional constitutive relations and earthquake nucleation. Chapter 2 briefly discusses the methodology. Chapter 3 focuses on demonstrating how the non-symmetric dipping on thrust and normal faults affects earthquake nucleation. Chapter 4 illustrates the effect of step-over features between the two parallel strike-slip faults on earthquake nucleation.

Chapter 2

Methodology

2.1 Fault Model Mechanics

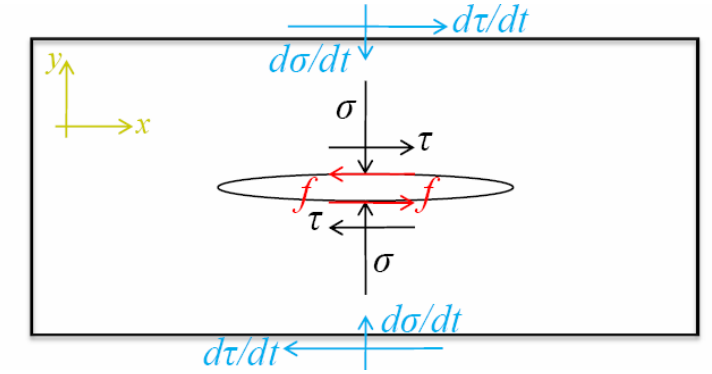

Figure 2-1. A schematic illustration of a 2D fault model. The fault is assumed to be a surface of displacement discontinuity in an infinite elastic medium. Fault slip is driven by external stressing rates $d\tau/dt$ and $d\sigma/dt$. In the following, fault is always under equilibrium conditions and shear stress τ is always balanced by friction f.

In our study, earthquake nucleation processes are modeled quasi-statically on simplified fault models. Faults are assumed as finite cracks imbedded in an infinite elastic medium and are loaded by remote stressing. Remote stressing causes relative displacement (fault slip) δ between the fault surfaces which induces friction. Shear stress τ along the fault interface is always balanced by friction f as $\tau = f$. Friction f also equals

friction coefficient μ times normal stress σ ($f = \mu\sigma$). Shear and normal stress τ and σ on the fault interface are given as

$$\tau = \tau_0 + \int \dot{\tau} dt + \Delta\tau, \sigma = \sigma_0 + \int \dot{\sigma} dt + \Delta\sigma \tag{2-1}$$

where τ_0 and σ_0 are initial shear and normal stress respectively. The integrations are stress changes resulted from remote stressing. For simplicity, remote stressing rate $\dot{\tau}$ and $\dot{\sigma}$ are always assumed to be independent of time so that the integrations can be simplified into simple products of stressing rate and the time elapsed Δt. $\Delta\tau$ and $\Delta\sigma$ represent shear and normal stress changes induced by fault slip δ. Calculation of $\Delta\tau$ and $\Delta\sigma$ analytically is always challenging even for 2D cases due to highly non-linear friction and complex fault geometry. Therefore, in our study, the whole elastic system is solved numerically by Boundary Element Methods (BEM). Two boundary element models based on different formulations have been developed and are elaborated in the following.

2.2 2D Plane Strain Formulation

Dieterich [1992] employed a plane strain model based on dislocation solutions in an infinite elastic medium. The formulation presented in *Dieterich* [1992] only applies to planar fault geometry from which fault slip will not cause normal stress variations. This formulation is not adequate for studying nucleation processes on geometrically complex faults. Therefore, we have extended the formulation to accommodate non-planar fault geometry.

Consider a fault with arbitrary geometry imbedded in an infinite elastic medium. The fault is discretized into n equally spaced segments. The normal displacement for every segment is always held zero under the assumption that faults will not open in the nucleation process. The tangential displacement (slip) δ on each segment is assumed constant. Therefore, there are displacement discontinuities at the boundaries of every segment, which are equivalent to edge dislocations.

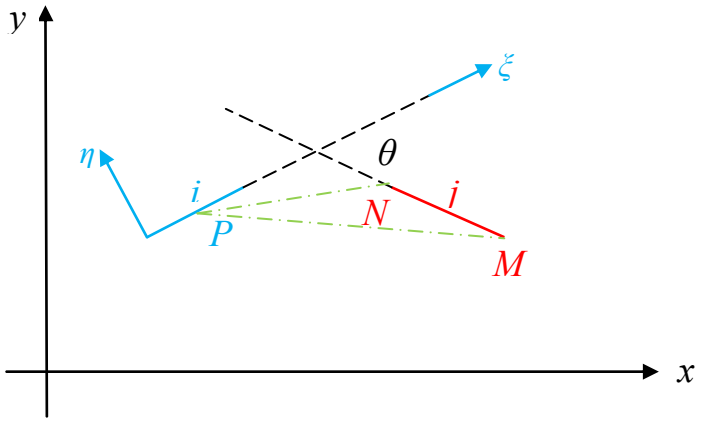

Figure 2-2. Dislocations at point M and N of element j exert shear and normal stress on element i which is evaluated at the center point P.

Denoting slip of element j as δ_j, then stress changes of element i ($\Delta\tau_i$ and $\Delta\sigma_i$) which is evaluated at the center point of the segment, can be calculated as

$$\begin{cases} \Delta\tau_i = \sum_{j=1}^{n} s_{ij}\delta_j \\ \Delta\sigma_i = \sum_{j=1}^{n} n_{ij}\delta_j \end{cases} \tag{2-2}$$

where s_{ij} and n_{ij} are interaction coefficients. Denoting the center point of element *i* as *P* and end points of element *j* as *M* and *N*, the interaction coefficients are given as

$$\begin{cases} s_{ij} = [\sigma_{\xi\eta}]_{PM} - [\sigma_{\xi\eta}]_{PN} \\ n_{ij} = [\sigma_{\eta\eta}]_{PM} - [\sigma_{\eta\eta}]_{PN} \end{cases} \tag{2-3}$$

where ξ and η are tangential and normal coordinates of element *i* as shown in Figure 2-2.

The stress terms in equation (2-3) can be calculated from 2D edge dislocation solutions in an infinite elastic medium. In a global coordinate (*x*, *y*), the stress field of an edge dislocation is given as

$$\begin{cases} \sigma_{xy} = \dfrac{G\delta}{2\pi\alpha} \dfrac{x(x^2 - y^2)}{(x^2 + y^2)^2} \\ \sigma_{xx} = -\dfrac{G\delta}{2\pi\alpha} \dfrac{y(3x^2 + y^2)}{(x^2 + y^2)^2} \\ \sigma_{yy} = \dfrac{G\delta}{2\pi\alpha} \dfrac{y(x^2 - y^2)}{(x^2 + y^2)^2} \end{cases} \tag{2-4}$$

where *G* is shear modulus and α equals $1-\nu$, where ν is Poison's ratio.

For general cases where faults are non-planar, element *i* and element *j* are not necessarily parallel to each other. Therefore, assuming the angle between element *i* and element *j* as θ (Figure 2-2), the stress at point *P* that is generated by the dislocation at point *M* is given as

$$\begin{cases} [\sigma_{xy}]_{PM} = \dfrac{G\delta}{2\pi\alpha}\dfrac{(x_p - x_m)[(x_p - x_m)^2 - (y_p - y_m)^2]}{[(x_p - x_m)^2 + (y_p - y_m)^2]^2} \\ [\sigma_{xx}]_{PM} = -\dfrac{G\delta}{2\pi\alpha}\dfrac{(y_p - y_m)[3(x_p - x_m)^2 + (y_p - y_m)^2]}{[(x_p - x_m)^2 + (y_p - y_m)^2]^2} \\ [\sigma_{yy}]_{PM} = \dfrac{G\delta}{2\pi\alpha}\dfrac{(y_p - y_m)[(x_p - x_m)^2 - (y_p - y_m)^2]}{[(x_p - x_m)^2 + (y_p - y_m)^2]^2} \end{cases} \tag{2-5}$$

Transforming the stress terms in equation (2-5) to local coordinate (ξ, η) gives

$$\begin{cases} [\sigma_{\xi\eta}]_{PM} = -\dfrac{[\sigma_{xx}]_{PM} - [\sigma_{yy}]_{PM}}{2}\sin 2\theta + [\sigma_{xy}]_{PM}\cos 2\theta \\ [\sigma_{\eta\eta}]_{PM} = \dfrac{[\sigma_{xx}]_{PM} + [\sigma_{yy}]_{PM}}{2} - \dfrac{[\sigma_{xx}]_{PM} - [\sigma_{yy}]_{PM}}{2}\cos 2\theta - [\sigma_{xy}]_{PM}\sin 2\theta \end{cases} \tag{2-6}$$

Stress at point *P* generated by the dislocation at point *N* can be derived in the same way as equations (2-5) and (2-6).

2.3 3D Variational Boundary Integral Formulation

In the framework of boundary integral equation methods, a crack is modeled as surface of displacement discontinuities in an elastic medium, and stress on the crack surface is related to the surface displacement via general solutions for dislocations in the half-space [e.g., *Chinnery*,1963]. The resulting integral equations are then solved by discretizing the crack surface with finite elements. In our study, we have incorporated both slip-dependent and rate- and state- dependent friction to a general variational boundary integral formulation of this type to study earthquake nucleation. The

formulation was developed for studying fracture mechanics and the development is described in detail in *Xu and Ortiz* [1993], *Xu et al.*, [1995], and *Xu* [2000].

Consider a general fault as displacement discontinuities $\boldsymbol{\delta}(\mathbf{x}, t)$ in an infinite elastic medium. The total energy of the system may be expressed as

$$\Pi[\boldsymbol{\delta}(\mathbf{x},t)] = W[\boldsymbol{\delta}(\mathbf{x},t)] + V[\boldsymbol{\delta}(\mathbf{x},t)] - P[\boldsymbol{\delta}(\mathbf{x},t)] \tag{2-7}$$

where W is the elastic strain energy, V is the potential energy associated with the constitutive relation, and P is the work done by remote tectonic loading. By modeling displacement as a continuous distribution of dislocation loops and using the expression of interaction energy between two dislocation loops [*Lothe*, 1982], the elastic strain energy W for anisotropic solids is given as [*Xu*, 2000]

$$\begin{aligned} W[\boldsymbol{\delta}(\mathbf{x},t)] = \frac{1}{16\pi^2} \int_S \int_S \frac{1}{R} \int_0^{2\pi} \mathbf{e}_j \cdot \{ & [(\mathbf{n} \times \nabla \delta_j)_i \times \mathbf{z}, (\mathbf{n} \times \nabla \delta_l)_k \times \mathbf{z}] - [(\mathbf{n} \times \nabla \delta_j)_i \times \mathbf{z}, \mathbf{z}] \\ & \cdot (\mathbf{z}, \mathbf{z})^{-1} \cdot [\mathbf{z}, (\mathbf{n} \times \nabla \delta_l)_k \times \mathbf{z}] \} \cdot \mathbf{e}_l \, d\varphi \, dS_1 \, dS_2 \end{aligned} \tag{2-8}$$

where S represents fault plane; $(\ )_i$ and $(\ )_k$ denote two different nodal points on fault plane; R is the distance between the two points; $\mathbf{e}_j$ and $\mathbf{e}_l$, j, l = 1, 2, 3, are Cartesian basis vectors; $\mathbf{n}$ is the unit normal of surface S while $\mathbf{z}$ is any unit vector in the plane perpendicular to R; φ is the polar angle of $\mathbf{z}$ within the plane. The components of the second-rank tensor in the notation $(\mathbf{a}, \mathbf{b})$ are defined as $(\mathbf{a}, \mathbf{b}) = a_i c_{ijkl} b_l$, where c_{ijkl} are elastic constants.

When slip-dependent friction is applied, the frictional potential energy V is an explicit function of fault slip $\boldsymbol{\delta}(\mathbf{x},t)$. Then the evolution of fault slip $\boldsymbol{\delta}(\mathbf{x},t)$ can be solved by rendering the total energy $\Pi[\boldsymbol{\delta}(\mathbf{x},t)]$ stationary, leading to an Euler equation that relates stress on the fault to displacements on the fault surfaces. The fault surface is discretized by triangular elements and the resultant nonlinear system of equations is solved with the Newton-Raphson method. This methodology has been employed by *Zhang et al.*, [2004, 2006] and the study presented in Chapter 3.

However, when rate- and state- dependent friction is applied, the frictional potential energy V is not solely dependent on fault slip δ. Therefore, the evolution of fault sliding conditions (displacement δ, slip rate v and state variable θ) can not be solved by rendering the total energy $\Pi[\boldsymbol{\delta}(\mathbf{x},t)]$ stationary. Instead, we have developed another way to solve the system which will be elaborated in section 2.4.

2.4 A Two Step Fixed Point Iteration Method

In the context of rate- and state- dependent friction, the evolution of fault slip, slip rate and state variable can be solved by a two step fixed point iteration method [*Dieterich*, 1992]. The method works surprisingly well and converges fast, usually requiring only three or four steps of iteration. The following text elaborates the details of the algorithm.

Assume we are at step i. The sliding condition at any specific element can be fully described by two parameters: the slip rate v_i and the state variable θ_i. To carry the computation to the next step, the following steps should be followed:

1) Set an initial guess of estimated friction coefficient μ at the middle point of next step denote by $\mu_{i+1/2}$. Simply, we can make $\mu_{i+1/2} = \mu_i$.

Iteration over j to find solution for step i:

2) Find a trial slip rate $v_{i+1/2}$ which is assumed constant over the time step. $v_{i+1/2}$ should satisfy that friction coefficient at the mid-point of the step equals current guess $\mu_{i+1/2}$. This requires iteration on rate- and state- dependent friction.

Iteration to find trial slip rate $v_{i+1/2}$:

<1> According to 'aging law' from equation (1-3) and assuming current slip rate v_i is constant over the step, the state variable at step i + ½ can be calculated as

$$\theta_{i+1/2} = \frac{D_c}{v_i} + (\theta_i - \frac{D_c}{v_i}) \exp(-\frac{\delta}{D_c}) \tag{2-9}$$

where δ is the accumulative slip from step 1. When normal stress is non-constant, the state variable evolves with the modified aging law shown by equation (1-5). The equation is an inhomogeneous first order ODE and can be solved numerically by fourth order Runge-Kutta method.

<2> According to rate- and state- dependent friction formulation shown by equation (1-2), once $\theta_{i+1/2}$ is known, slip rate $v_{i+1/2}$ can be calculated as

$$v_{i+1/2} = v^* \exp(\frac{\mu_{i+1/2} - \mu_0}{a})(\frac{\theta_{i+1/2} v^*}{D_c})^{-b/a} \tag{2-10}$$

End of iteration to find trial slip rate $v_{i+1/2}$.

3) Employ the resulting trial slip rate $v_{i+1/2}$ to get the trial slip displacement as $\delta_{i+1/2} = \delta_i + v_{i+1/2}\Delta t/2$ (Δt is current time step). Once $\delta_{i+1/2}$ is known, the change of shear and normal stress $\Delta\tau_{i+1/2}$ and $\Delta\sigma_{i+1/2}$ can be calculated by timing the stiffness matrix K with the trial slip vector $\boldsymbol{\delta}_{i+1/2}$. This gives a new estimation of the friction coefficient $\mu_{i+1/2}$ $= (\tau_0 + \Delta\tau_{i+1/2})/(\sigma_0 + \Delta\sigma_{i+1/2})$.

4) Test for convergence based on $\left|(\mu_{i+1/2}^{j+1} - \mu_{i+1/2}^{j})/\mu_{i+1/2}^{j}\right| = test$, $\mu_{i+1/2}^{j}$ and $\mu_{i+1/2}^{j+1}$ are friction coefficients at iteration steps j and $j + 1$ at time step i. If *test* is greater than the convergence criterion, then use $\mu_{i+1/2}^{j+1}$ to start step (2) again iteration $j + 2$. If *test* is smaller than convergence criterion, then use current $v_{i+1/2}$ to advance solution to step $i + 1$.

End iteration over j at time step i.

5) Since slip rate is assumed constant over the time step i, then $v_{i+1/2} = v_{i+1}$. θ_{i+1} can be calculated from equation (2-9) with the cumulative displacement $\delta_{i+1} = \delta_i + v_{i+1}\Delta t$ when normal stress is constant. If normal stress is non-constant, θ_{i+1} can be solved by Runge-Kutta method with known Δt and v_{i+1}.

6) Repeat from step **(1)** for time step $i + 1$.

Another advantage for using this method is that unlike the Newton-Raphson method, this method do not requires inverse of the stiffness matrix **K,** which greatly reduces the computational time. For Newton-Raphson method, the computational time is

proportional to n^3 (n is the rank of the stiffness matrix **K**) while for the two step fixed point iteration method, the computational time is only proportional to n^2.

Chapter 3

Earthquake Nucleation on Bent Dip-Slip Faults

3.1 Introduction

The events and interactions that lead to the initiation of unstable fault slip are collectively defined as earthquake nucleation. It is a mechanical process influenced by fault geometry, frictional properties, initial conditions, and loading. Understanding this process is of fundamental importance because it may lead to better predictions of hypocenter location and occurrence time of earthquakes, which in turn affect spatio-temporal patterns of seismicity. Direct studies of earthquake nucleation in nature are difficult, as nucleation takes place well below the earth's surface, at a slow pace, with little or no seismic signal. Many studies of this process therefore rely on computational models using friction laws inferred from laboratory experiments [e.g., *Dieterich*, 1986; *Dieterich*, 1992; *Rice*, 1993; *Stuart and Tullis*, 1995; *Kato and Hirasawa*, 1997; *Shibazaki*, 2002; *Lapusta and Rice*, 2003; *Zhang et al.*, 2004; *Rubin and Ampuero*, 2005; *Zhang et al.*, 2006; *Ampuero and Rubin*, 2008]. Typically, nucleation starts with a slow quasi-static slip phase followed by a phase of slip acceleration over a small region, and the subsequent onset of unstable rupture propagation over a large area. The details of nucleation location, time, and size can vary considerably as a result of differences in

model configurations, frictional properties, initial and loading conditions [*Dieterich*, 1992; *Rubin and Ampuero*, 2005; *Ampuero and Rubin*, 2008].

Previous studies have also been largely focused on nucleation on single planar faults with slip weakening or rate- and state-dependent frictional properties. Natural fault systems, however, are rarely perfectly planar, but rather have non-planar features such as bends, stopovers, and branches [e.g., *Wesnousky*, 1988; *Zachariasen and Sieh* 1995; *Zoback et al.*, 1999; *Zampier et al.*, 2003; *Brankman and Aydin*, 2004].

Non-planar fault geometry is known to have a large effect on earthquake rupture dynamics and co-seismic slip. Fault bends, branches and step-overs can have a strong effect on rupture propagation and slip distribution, which can consequently cause stress buildups and reductions near these geometric irregularities [*Harris et al.*, 1991; *Harris and Day*, 1997; *Bouchon and Streiff*, 1997; *Nielsen and Knopoff*, 1998; *Magistrale and Day*, 1999; *Harris et al.*, 2002; *Poliakov et al.*, 2002; *Kame et al.*, 2003; *Oglesby and Archuleta*, 2003; *Oglesby et al.*, 2003a, 2003b, *Oglesby*, 2005, 2008; *Duan and Oglesby*, 2005, 2007]. Non-vertical dipping faults induce an asymmetry between the motion on hanging wall and foot wall, as well as an amplification of thrust fault motion in comparison to normal fault motion [*Brune*, 1996; *Nielsen*, 1998; *Oglesby et al.*, 1998; *Shi et al.*, 1998; *Brune and Anooshehpoor*, 1999; *Oglesby et al.*, 2000a, 2000b; *Aagaard et al.*, 2001; *Oglesby and Day*, 2001b, 2001a]. In all these cases, the complexities in rupture propagation, fault slip and ground motion are caused by complex fault geometry. It is very possible that fault geometrical complexities can have large effects not only on the

transient rupture dynamics but also on the long term quasi-static nucleation processes which has already confirmed by a few recent nucleation studies on geometrically complex faults. For example, *Nielsen and Knopoff* [1998] studied the effect of repeated ruptures on a non-planar fault system using a quasi-static model. They found that extensional stopovers were common places for earthquake occurrence, as expected from the reduced yield stress in these locations.

In addtion, our previous studies of earthquake nucleation on planar dip-slip faults [*Zhang et al.*, 2004, 2006] have demonstrated that normal stress variation caused by breaking down of fault symmetry with respect to the Earth's surface has a significant influence on both the location and timing of earthquake nucleation on both thrust and normal faults. Since natural dip-slip faults are usually non-planar with dip angles that change with depth, this non-planar geometric feature is expected to influence the normal stress distribution on dip-slip faults even more significantly than the cases with planar fault plane. In this chapter, we focus on earthquake nucleation process on dip-slip faults with changes in dip angle. For simplicity, we only consider a bend half-way down the fault plane (i.e. the two fault segments have different dip angles). The goal is to investigate how the bend affects the location and occurrence time of earthquake nucleation.

3.2 Fault Model Configuration

We assume a two-dimensional segmented dip-slip fault that intersects Earth's surface, as illustrated in Figure 3-1. The dip angles of the upper and lower fault segments are denoted by α_1 and α_2 respectively. For simplicity, α_1 is fixed to be 45°, while α_2 is variable. We note that the effect of the dip angle of the shallow segment with respect to the Earth's surface (α_1) is investigated in detail in *Zhang et al*. [2004; 2006]. The bend angle is denoted by β (with sign defined in Figure 3-1) which equals to the difference between the dip angles of the two fault segments:

$$\beta = \alpha_1 - \alpha_2,\ \alpha_1 = 45^\circ,\ \ \alpha_2 \in (0, 90^\circ) \tag{3-1}$$

The down-dip lengths of the two fault segments are denoted by L_1 and L_2, respectively, and are each fixed to be 10 km. The Cartesian coordinates are selected so that the z-axis is normal to earth's surface, the y-axis is along the intersection of the fault and earth's surface, and the x-axis is perpendicular to strike, positive along the hanging wall.

The lithosphere is approximated to be a homogeneous linear elastic plate lying on top of a relaxed asthenosphere that accommodates relative displacement caused by tectonic loading plastically. We approximate tectonic loading by imposing a uniform slip rate $V_{base} = 1\times10^{-9}$m/s at the base of the fault, in a manner similar to that of *Rice* [1993]. For simplicity, we use a plane strain configuration, i.e., the displacement and shear stress on the slip plane are assumed to be uniform along the y-axis. Furthermore, homogeneous (depth-independent) stress and frictional properties are assumed so that we may isolate the effects of fault geometry. We note that depth-dependent friction can be readily implemented in the model [*Zhang et al.*, 2006].

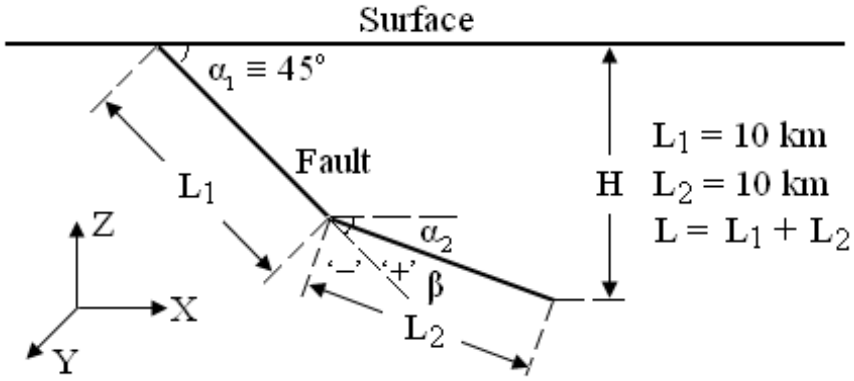

Figure 3-1. Schematic diagram of fault configuration. The fault has two segments with the same down-dip length but different dip angles. The dip angle of the upper segment α_1 is fixed to be 45°, while the dip angle of the lower segment α_2 is variable. The total down-dip length of the fault is denoted by L, and the vertical depth of the fault is represented by H. The difference of the dip angles of the two fault segments is defined as the bend angle, denoted by β, and its sign is illustrated in the figure.

3.3 Frictional Constitutive Relations

The occurrence of unstable slip on a fault critically depends on the frictional constitutive relation along the fault. We use a non-linear slip dependent friction constitutive relation simplified from a rate- and state-dependent formulation [*Dieterich*, 1979, 1981; *Ruina*, 1983]. This numerical method is the same as that of *Zhang et al.*, [2004; 2006]. Thus we describe our methodology only briefly here. To incorporate variability of normal stress on dip-slip faults, the frictional stress τ along the fault is expressed as

$$\tau = \mu(\sigma_{\mathrm{n}} - \Delta\sigma_{\mathrm{n}}) \tag{2-2}$$

where σ_n is the ambient effective normal stress on the fault, $\Delta\sigma_n$ is the its variation, and μ is friction coefficient, which in turn is expressed as

$$\mu = \mu_0 + \Delta\mu f(\delta_r) \tag{2-3}$$

where μ_0 is the initial friction coefficient, $\Delta\mu$ is the maximum variation of the friction coefficient, and δ_r denotes the relative shear displacement along the fault surfaces. The function $f(\delta_r)$ represents the displacement-dependent strengthening and weakening frictional process, which is modeled by

$$\begin{cases} f(\delta_r) = \dfrac{\delta_r}{\delta_{rc}} \exp\left(1 - \dfrac{\delta_r}{\delta_{rc}}\right), & \delta_r < \delta_{rc} \\ f(\delta_r) = \exp\left(-\dfrac{\delta_r - \delta_{rc}}{L_c}\right), & \delta_r > \delta_{rc} \end{cases} \tag{2-4}$$

where δ_{rc} is the critical displacement at which friction reaches its peak value and L_c is the characteristic length corresponding to the weakening process.

To accommodate the variability of normal stress, we apply the penalty method from *Zhang et al.*, [2004; 2006], which introduces an imaginary spring between the fault surfaces in the normal direction. This penalty method is widely used in structure analysis to avoid the difficulty that normal stress is a step function of normal displacement [*Hughes*, 1987]. The stress and displacement relation of the spring is expressed by

$$\Delta\sigma_n = \sigma_n\left[1 - \exp(-\delta_n/\delta_{nc})\right] \tag{2-5}$$

where δ_n is the relative normal displacement of the fault surfaces and δ_{nc} is the characteristic displacement. The characteristic behavior and numerical advantages of the above relation have been described in detail in *Zhang et al.*, [2004; 2006].

In the present study we use the same numerical method as *Zhang et al.*, [2004; 2006]. Faults are modeled as surfaces of displacement discontinuity in an elastic medium, and the stresses on the faults are related to the relative fault displacements through boundary integral equations as described in section 2.3. The evolution of fault slip $\boldsymbol{\delta}(\mathbf{x},t)$ is solved numerically by rendering the total energy of the system stationary through the variational principle. This formulation in principle is applicable only to a fault system

embedded in an infinite elastic medium. To include the effect of the earth's surface, we adopt the approach described in *Xu and Zhang* [2003] which allows for the use of the formulation for half space problems. In this approach, the earth's surface is modeled as part of a very large open crack embedded in an infinite solid. This crack is chosen be much larger than any relevant size of the fault configuration, transforming the problem into an equivalent system that is essentially composed of the fault and the crack (free surface) embedded in an infinite solid. A uniform slip rate boundary condition at the bottom of the fault is enforced by Lagrange multipliers. Δt is the adaptive time step that is adjusted according to the maximum slip rate on the fault, so that the maximum slip displacement increment on the fault at each step does not exceed a critical value. The computation stops when the maximum slip rate becomes infinitely large, and the time step becomes infinitely small, corresponding to slip instability at the location where maximum slip rate occurs.

3.4 Results

1. General effects of fault geometry on stress

When the fault in Figure 3-1 is subjected to displacement loading at the fault base, a positive bend on the thrust fault and a negative bend on the normal fault both serve as barriers to the relative motion on upper fault segment. In both of these cases, (aseismic) slip on the lower segment increases the clamping normal stress on the upper segment, resulting in a stronger upper fault segment, especially in the vicinity of the bend (note

that in the following discussion, we follow the geological convention and refer to increased compressive stress on a fault as an 'increase' in normal stress, even though our equations above and our figures follow the engineering sign convention of normal stress being positive in extension). Conversely, a negative bend on the thrust fault and a positive bend on the normal fault tend to unclamp the upper fault segment as the lower segment slips, resulting in a weakened region on the upper fault segment. In principle, singular stress is expected to result from this abrupt change of fault geometry because the stress is not relaxed in our elastic model with a geometrical discontinuity. The extreme stress built up, however, appears to be quite localized, and has little significant effect on the overall results in this study. We have verified this impression by smoothing the sharp bend with a curved fault linking the two planar fault segments. The bend can be either smoothed locally over a small region, or in an extreme case the entire fault plane can become smoothly curved like a listric fault, with a continuous change of dip angle. A small smoothed region still results in large stress buildup with less severity compared to the case with a sharp kink, while the continuously curved fault completely smoothes out the stress concentration. We carried out a number of simulations for faults with a sharp bend and for faults with a locally smoothed bend. The results indicated that although there are quantitative differences near the bends, the basic pattern of the evolution of peak slip rate (described in detail below) remains, suggesting that a sharp bend can be an adequate representation of the abrupt change of dip angle on different segments of dip-slip faults. In the following results, we choose to represent the bent dip-slip faults with sharp bends for simplicity.

2. Time-dependent stress perturbations

First, we consider two faults with medium bend angle, $\beta = \pm 10^{o}$. With the dip angle of the upper segment fixed as $\alpha_1 = 45^{o}$, the dip angles of the lower segment in these two cases are thus $\alpha_2 = 35^{o}$ and $\alpha_2 = 55^{o}$ respectively. We model the faults with following parameters: $L_1 = L_2 = 10$ km, $\mu_0 = 0.6$, $\Delta\mu = 0.02$, $L_c = 20$ cm and $\delta_{rc} = 10$ cm, consistent with our earlier work on dip-slip faults [*Zhang et al.*, 2004, 2006]. Sequential snapshots of variation in shear and normal stress (scaled to the initial shear stress) on the bent normal and thrust faults are shown in Figures 3-2 and 3-3, compared with corresponding results for planar faults. In the figures that describe the along-fault distribution of variables, the horizontal axis represents the along-fault distance, denoted by r, from the earth's surface, scaled by the fault length L. Hence, a zero value of r/L corresponds to earth's surface, while $r/L = 1$ corresponds to the deepest extent of the fault. Due to the basal loading, at first, shear stress gradually builds up near the base. This build-up is then followed by a stress drop as the bottom part of the fault begins to slip and traverse to the slip-weakening path. The shear stress peak migrates up-dip toward the earth's surface, taking the form of a quasi-static rupture front. It is important to note that this 'rupture front' is slow-moving. It does not correspond to an earthquake, and takes place prior to the onset of slip instability. For planar faults [Figures 3-2(a1 and b1) and 3-3(a1 and b1)], the effects of the non-vertical fault geometry can be summarized as: normal faults are

unclamped near the surface and clamped at depth, while thrust faults are clamped near the surface and unclamped at depth. For nonplanar faults there are significant variations from this pattern near the bend as preseismic slip propagates upward toward the earth's surface. On bent thrust faults with a positive bend angle [Figure 3-2(b3)], The stress peak increases dramatically on the up-dip side of the bend compared to that of a planar thrust fault, suggesting the fact that the upper segment of the fault is clamped and strengthened by slip below the bend [Figure 3-3(b3)]. Conversely, the bend with the negative angle weakens the upper segment of the thrust fault [Figure 3-2(b2), Figure 3-3(b2)]. For normal faults, the bend has an opposite effect: slip on the basal fault clamps down and strengthens the upper segment in the case of a negative bend angle, and unclamps and weakens the upper segment in the case of a positive bend angle. Below the bend, we can also observe the feedback of upper-segment slip to the lower segment: Bends with negative angles clamp down and strengthen the lower segment of thrust faults, while they unclamp and weaken the lower segment of normal faults. However, bends with positive angles have the opposite effects.

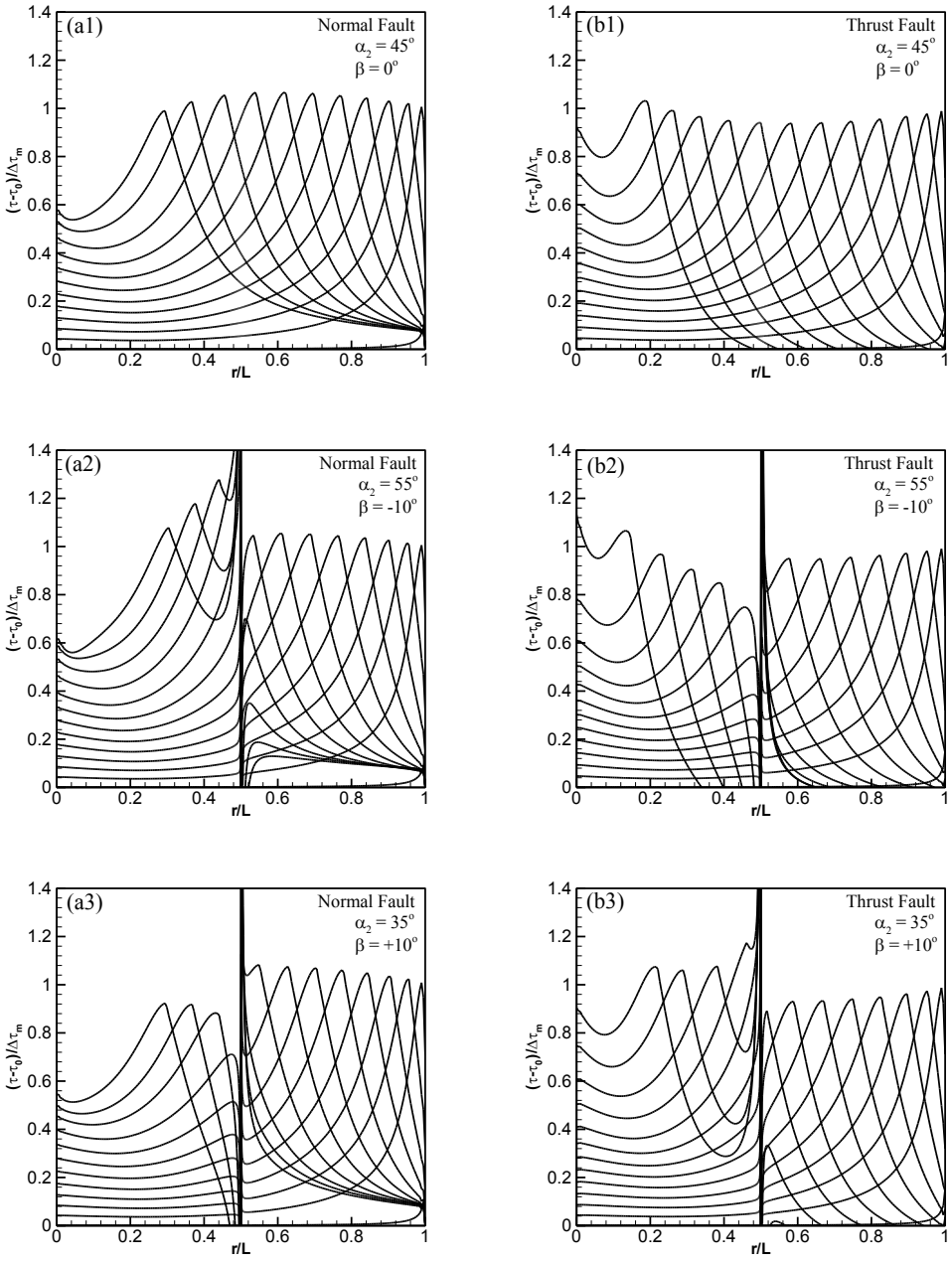

Figure 3-2. Sequential snapshots of variation of shear stress before nucleation on normal faults (a1, a2, a3) and thrust faults (b1, b2, b3). Due to the different direction of slip at the base, as well as the effect of the bend, shear stress variations are strongly altered from those on planar faults.

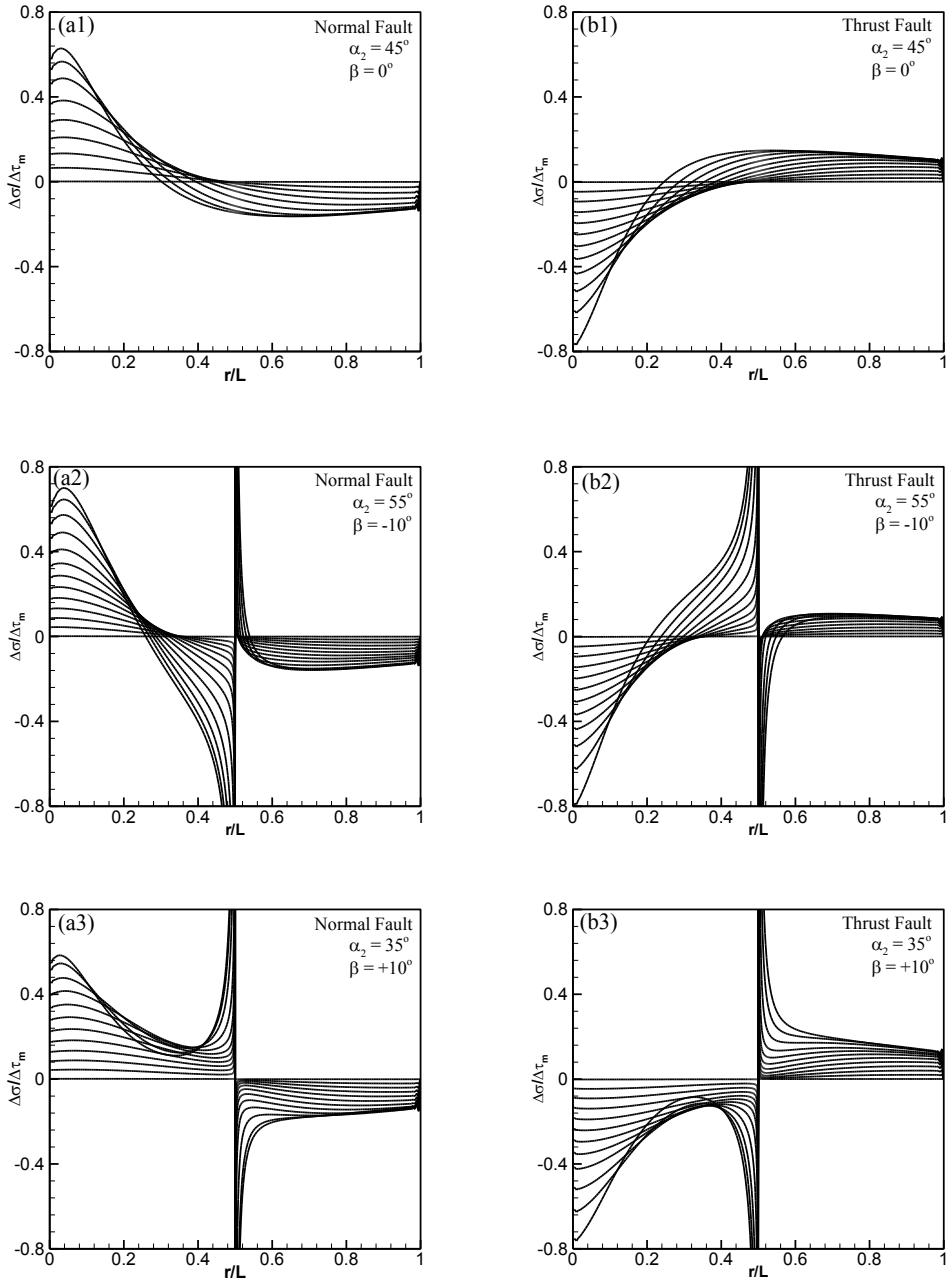

Figure 3-3. Sequential snapshots of variation of normal stress before nucleation on normal faults (a1, a2, a3) and thrust faults (b1, b2, b3). The fault geometry produces a significant effect in the normal stress evolution.

3. Effect of fault bend on slip rate evolution and nucleation

Our results have shown that both the non-vertical fault geometry and the bend of the fault plane manifest their roles in the evolution of slip rate (Figure 3-4). For planar thrust and normal faults (Figure 3-4(a1) and 3-4(b1)), in the early stages of the nucleation process, most of the fault is locked, with a much smaller slip rate than the loading rate at the base (which equals 1 in these scaled diagrams). As time elapses, slip rate gradually increases in a pattern that migrates up-dip from the fault base. Eventually, a region of high slip rate localizes and follows the quasi-static rupture front migrating up-dip, taking the form as a nucleation patch. Fault slip rate evolves continuously and increases monotonically during the entire nucleation process.

For bent faults, however, there are spatially abrupt changes of slip rate at the bend, and in many cases the slip rate at each point on the fault does not increase monotonically. For example, in the case of normal fault with a negative bend (Figure 3-4(a2)), slip at depth induces clamping of the upper fault segment, which slows the progression of the quasi-static rupture front and produces a discontinuity in fault slip rate at the bend. The slower migration speed of the quasi-static rupture front implies that while the high-slip-rate-patch is being held at the bend, the deeper part of the fault traverses its slip-weakening curve, and slows down; slip velocity is no longer monotonic here. Almost the same process takes place for the thrust fault with a positive bend (Figure 3-4(b3)) which is due to a similar clamping effect on the upper fault segment. Interestingly, nucleation process normal fault with a positive bend and thrust fault with a negative bend evolves

quite differently. Normal faults with a positive bend experience a monotonic slip velocity increase everywhere, but with a discontinuity at the bend caused by clamping of the lower segment from upper segment slip. Thrust faults with a negative bend, however, experience a stronger effect from the non-planar fault geometry: the quasi-static rupture front speeding up and slowing down in a rather complicated way as it migrates up-dip. This effect can be best interpreted by analyzing the evolution of peak fault slip rate, as shown in Figures 3-5 and 3-6.

The influence of the bend on nucleation location and time for both thrust and normal faults is shown in Figures 3-5 and 3-6, in which the evolution of the peak slip rate is plotted as a function of down-dip location in (a) and total accumulation of slip at the fault base in (b). The horizontal coordinate that corresponds to divergent slip velocity represents the down-dip location of nucleation in Figures 3-5(a) and 3-6(a), and the time of nucleation in Figure 3-5(b) and 3-6(b). In cases with planar fault geometry, peak slip rate migrates up-dip along with the quasi-static rupture front, and eventually reaches instability at the location of nucleation. Also, peak slip rate increases monotonically with time. This pattern is quite different from the cases with complex fault geometry.

For thrust faults with a negative bend (Figure 3-5(a)), the magnitude of peak slip rate first increases as it migrates upward. The increase is faster than that in cases with planar fault, perhaps because the unclamped upper segment experiences a higher slip rate which pulls the lower segment along. After peak slip rate reaches the bend, it slows down due to clamping of the lower segment and results in suppression of slip for a long time

period. However, for the case studied, peak slip rate managed to migrate into the upper fault segment on which it increases rapidly and reaches instability in a very quick manner. Compared to planar fault cases, the resulting nucleation location is closer to the earth's surface, while the change in the occurrence time is quite small. We note that the nearly identical nucleation time is merely a coincidence for this special case. Nucleation time will be quite different for other bend angles as it compared to the planar cases. For thrust faults with a positive bend angle, peak slip rate starts to decrease as it migrates upward due to the clamping of the upper segment and the resultant suppression of slip; it becomes even smaller than the basal loading rate as the peak slip rate patch approaches the bend. The peak slip rate is reduced between symbols X and O as shown in Figure 3-5(a) and 3-5(b). During this period, the displacement at the fault base is approximately 1.5×10^{-5}, corresponding to about 10 years if a typical basal slip rate of $1x10^{-9}$m/s is assumed. Because of this delay, it takes more time for stress to build up on the lower segment so that the high slip rate patch can migrate into the upper segment. Once the peak slip rate patch migrates to the upper segment, however, it takes a relatively short time for the patch to accelerate to instability. Thus, in this case, earthquake nucleation is delayed relative to nucleation on planar faults, but takes place farther down-dip.

Figure 3-6 shows a somewhat similar pattern for evolution of peak slip rate on normal faults. For normal faults with a negative bend angle, nucleation evolves in a way that is similar to that on thrust faults with a positive bend angle: clamping of the upper segment slows down the advancement of the peak slip rate patch, leading to reduced slip rate for a significant time period, and delayed earthquake nucleation for a substantial

amount of time. Conversely, normal faults with a positive bend angle experience increased slip rate and an earlier rupture nucleation. For normal faults with this set of bend angles, nucleation location seems not sensitive to bend geometry.

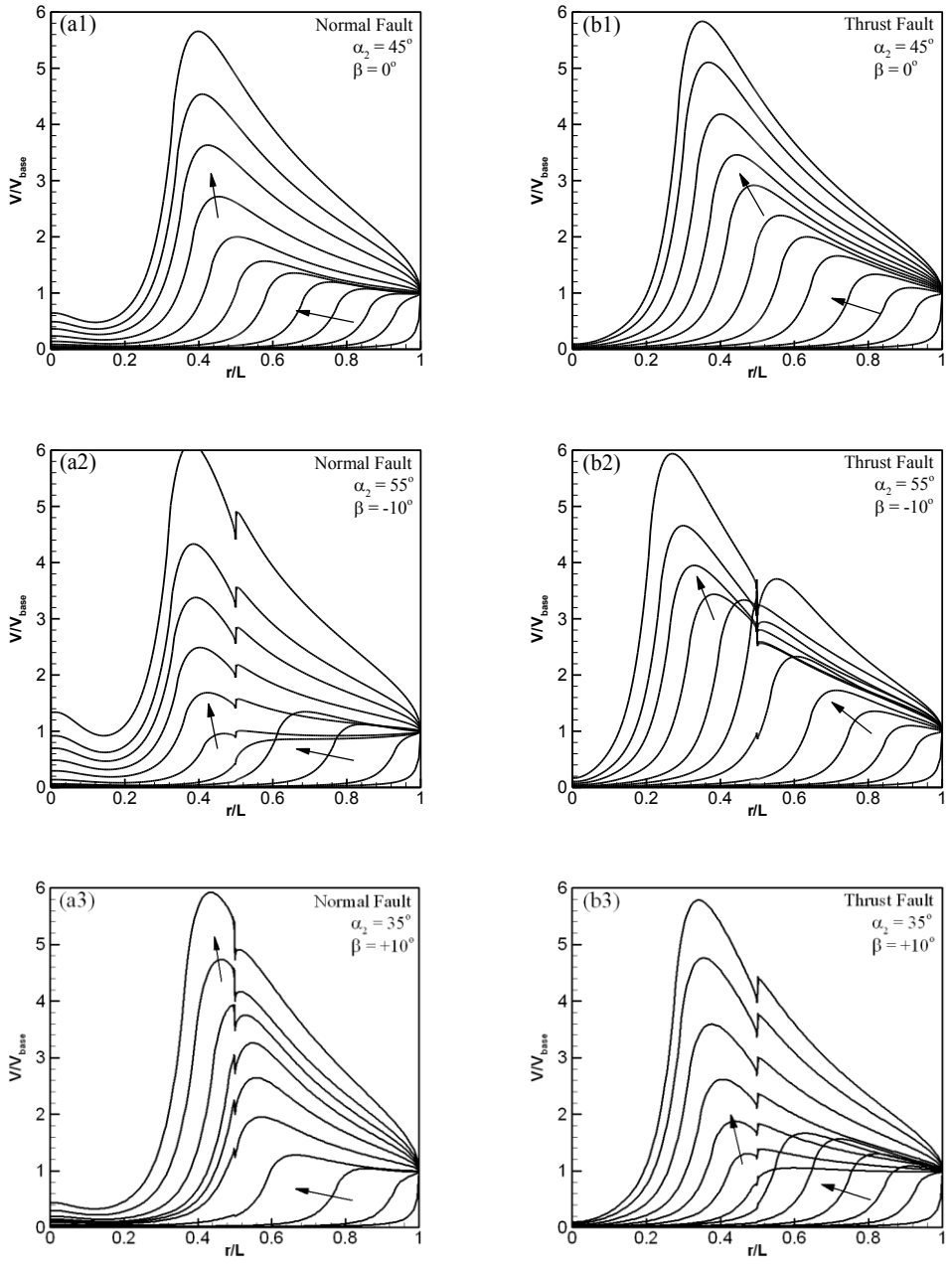

Figure 3-4. Sequential snapshots of slip rate (normalized with displacement loading rate from the base) before nucleation on normal faults (a1, a2, a3) and thrust faults (b1, b2, b3). A stress discontinuity at the bend leads to a corresponding slip rate discontinuity, along with non-monotonically increasing slip rate with time. Arrows indicate the flow of time.

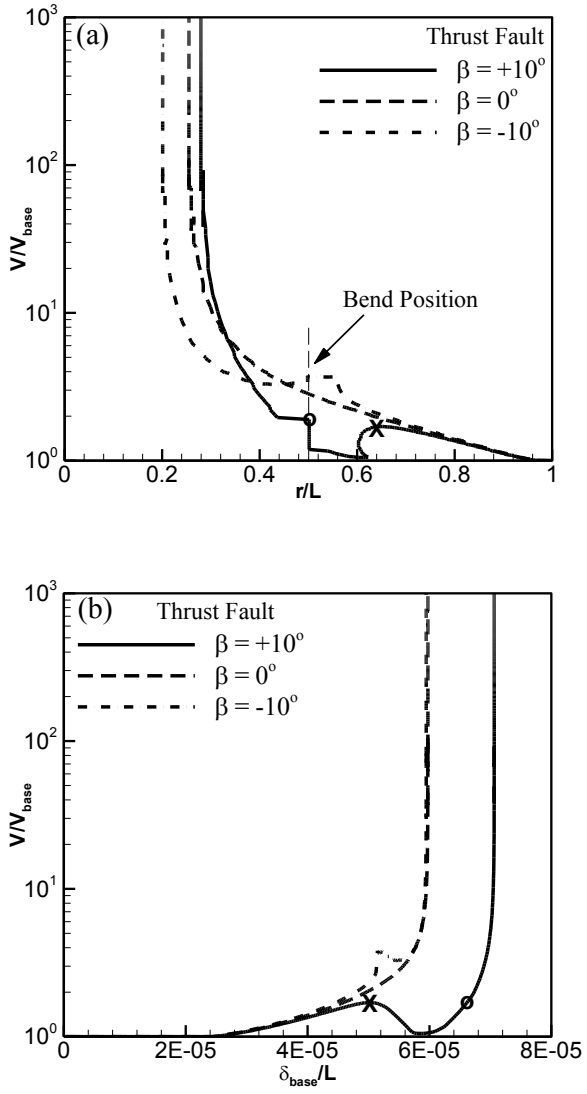

Figure 3-5. Peak slip rate on bent thrust faults with positive and negative bend angles (a) as a function of down-dip distance and (b) as a function of the base displacement (a proxy of time). For the horizontal axis in (a), 0 corresponds to earth's surface, 0.5 denotes the bend, and 1 refers to the down dip edge of the lower fault segment. Divergence of the slip rate corresponds to the onset of unstable slip. The evolution of peak slip rate is altered both spatially and temporally due to the strong local effect caused by the bend.

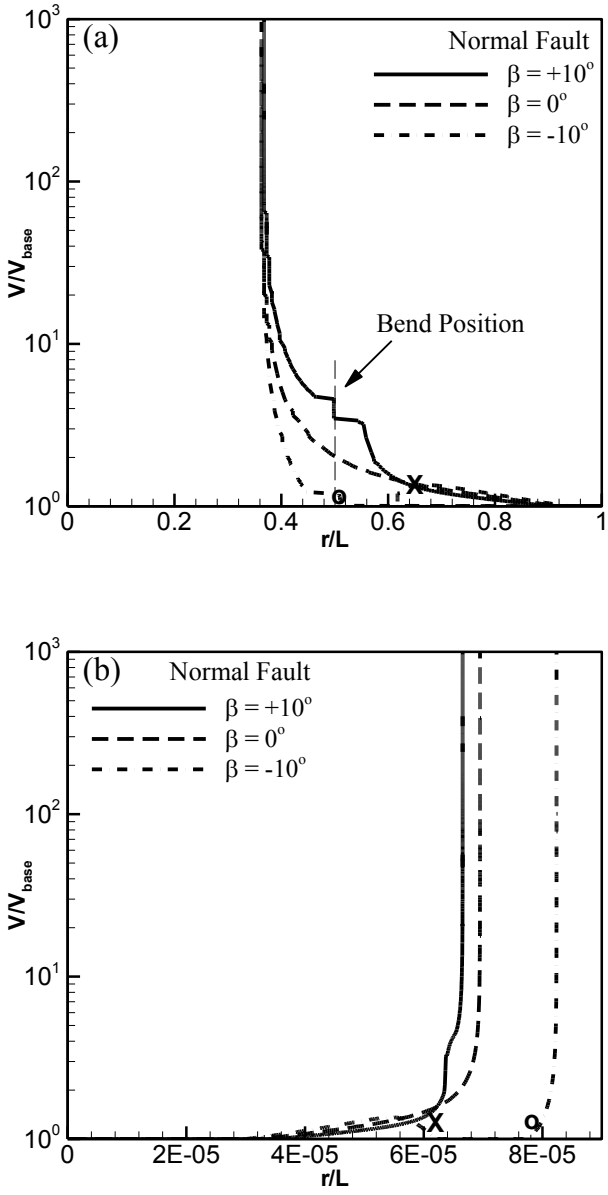

Figure 3-6. Peak slip rate on bent normal faults with different bend angles (a) as a function of down-dip distance, and (b) as a function of the base displacement (a proxy for time). Axes are the same as Figure 3-5. Similar as the cases with thrust faults, the peak slip rate evolution is altered both spatially and temporally by the bend.

4. Summary results for variable fault bend

To generalize the effect of bend angle on nucleation location and time, we model a family of thrust and normal faults with bend angles ranging from −40° to 40°. The dip angle α_1 of the upper fault segment is still fixed at 45°, while the dip angle of lower segment α_2 ranges from 5° to 85°; i.e., the lower fault plane ranges from nearly horizontal to nearly vertical. In Figure 3-7, we plot earthquake nucleation location as a function of the bend angle for both normal and thrust faults. For thrust faults, the relationship is relatively simple. Earthquakes always nucleate on the upper fault segment, and the hypocenter becomes shallower as the lower segment becomes steeper. For normal faults, the relationship is more complicated. When the bend angle is larger than −15°, corresponding to a dip angle α_2 smaller than 60°, earthquakes nucleate in roughly the same region, about 7~8km down dip along the upper fault segment. Nucleation locations change dramatically and become much deeper as the bend angle becomes more negative than −15° and eventually, earthquakes are nucleated on the lower segment when the bend angle is less than −20° (i.e., for a very steep lower segment). The effect of dip angle on nucleation timing is also significant. Figure 3-8 shows the relationship between the base displacement before instability (a proxy for nucleation time) and the bend angle for both thrust and normal faults. A large bend angle, either positive or negative, can delay the onset of earthquakes significantly. Earthquakes on thrust faults with a nearly horizontal lower segment take much more time (about 10 times longer) to nucleate than those on planar faults. One interesting phenomenon is that the shortest nucleation time does not occur on planar faults for either fault type. Instead, the quickest nucleation happens when

there is a small bend about 10°, negative for thrust faults and positive for normal faults. The reason for this phenomenon may be that the Coulomb stress changes reach maximum at this two bend angles which promotes faster nucleation as suggested by *Fang et al.*, [2009b].

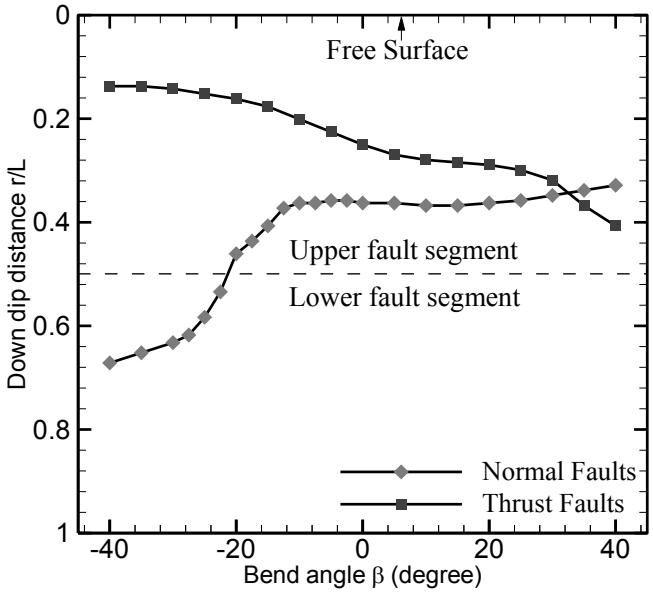

Figure 3-7. Nucleation location as a function of bend angles for normal and thrust faults. Dashed line corresponds to the down-dip location of the bend.

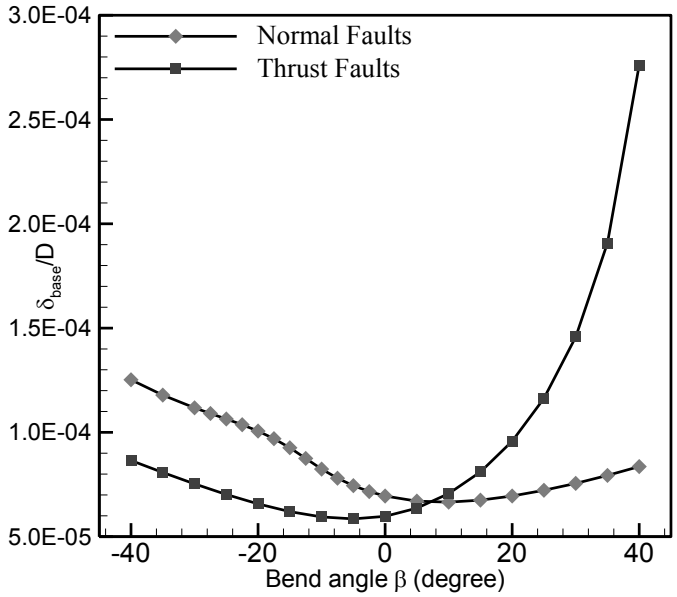

Figure 3-8. Base displacement before instability as a function of bend angle for both thrust and normal faults. When external loading rate is constant, the base displacement indicates the time to instability. Nucleation time on both types of faults increases as the absolute value of the bend angle increases. The time to instability for nucleation on thrust faults is more sensitive to the bend angle than that on normal faults. The shortest nucleation time does not occur on a planar fault for either type of fault.

3.5 Discussion

The location and timing of earthquake nucleation are both strongly affected by the presence of a bend on a dip-slip fault. The existence of a bend changes normal stress on the fault, feeding back to the fault friction via the direct relationship between friction and normal stress. For thrust faults, the nucleation location migrates up-dip as the lower segment becomes steeper. This effect can be understood as a consequence of earthquake nucleation preferentially taking place in a location with higher normal stress, where the stress drop is larger, and consequently the critical patch size for the formation of instability is smaller.

The pattern is more complicated for normal faults. For bend angles more negative than around 15°, the nucleation location migrates down-dip due to increased clamping of the upper segment near the bend, consistent with the thrust fault case. However, at a bend critical angle, the clamping of the upper segment of the normal fault becomes so extreme that the quasi-static rupture front cannot proceed to the upper segment. Figure 3-9 shows the sequential snapshots of variation of shear stress when β equals $-25°$. With the shear stress peaks representing the migrating quasi-static rupture front, we can observe that there is no progression of the shear stress peak above the bend, so nucleation is confined to the lower segment.

The result that earthquake nucleation preferentially occurs in areas of increased clamping stress appears to be in conflict with the work of *Duan and Oglesby* [2005], who

found that earthquake nucleation on nonplanar strike-slip faults was preferentially at locations of reduced, rather than increased normal stress. However, this prior study uses significantly different assumptions and methodology than the current study. In particular, *Duan and Oglesby* [2005] did not rigorously model the nucleation process, and held the critical patch size for nucleation artificially constant. Additionally, the current work starts with homogeneous initial stress, whereas the heterogeneous stress in *Duan and Oglesby* [2005] was the result of prior earthquakes and loading in the system. More work must be done to investigate this apparent conflict; such work will likely require more accurate frictional parameterizations such as full normal-stress-dependent rate-state [*Linker and Dieterich*, 1992] as well as modeling of multiple seismic cycles.

The effect of bend angle on nucleation time may also be quite significant. Since the energy released by earthquakes is proportional to the time between two earthquakes if the loading rate is constant, the delay of nucleation time may imply that a large bend on a dip-slip fault can lead to a potentially larger earthquake. Nevertheless, as shown in Figure 3-8, the minimum nucleation time on both normal and thrust faults does not occur on planar faults. As shown in Figure 3-6(b), when the bend angle on a normal fault is 10°, the peak slip rate develops much faster as it approaches and passes the bend. In this case, the upper fault segment is being unclamped; allowing the quasi-static rupture front to precede up-dip rapidly, but it is not unclamped so severely that nucleation is delayed. A similar argument can be made for the thrust faults at a bend angle of around −7°.

Although the bend can play a significant role in the nucleation process, the Earth's surface is still clamped for thrust faults and unclamped for normal faults [*Zhang et al.*, 2004; *Zhang et al.*, 2006]. In agreement with work on planar faults, the preseismic surface slip on normal faults is larger than those on thrust faults, and almost all of the earthquakes on thrust faults with different bend angles still nucleate farther up-dip than on equivalent normal faults. This overall result suggests that the basic behavior of normal and thrust fault are largely by the asymmetrical geometry and sense of slip, but are strongly modulated by the deeper geometry.

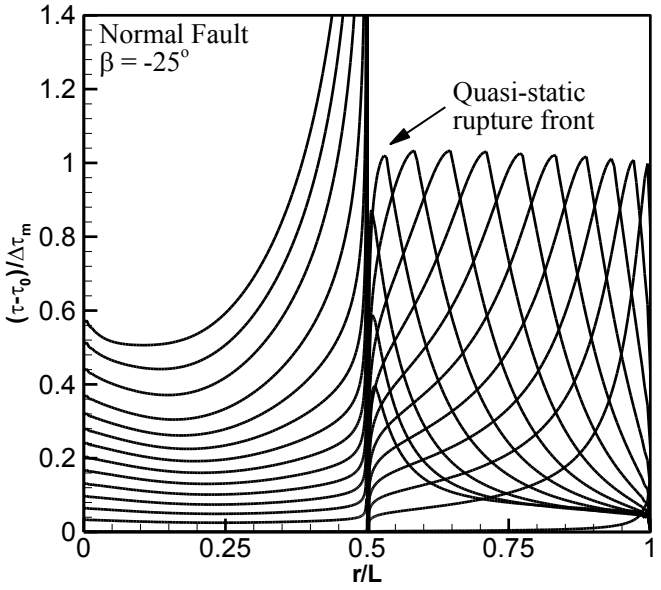

Figure 3-9. Sequential snapshots of variation of shear stress before nucleation on a strongly bent normal fault with bend angle −25°. The deeper part of the upper fault segment is strongly clamped by the bend, so the quasi-static rupture front, denoted by the upward moving peaks of shear stress, is halted at the bend, forcing nucleation to take place on the lower segment.

3.6 Conclusion

We have previously shown that the asymmetric geometry of planar dip-slip faults can have a significant effect on the nucleation process on both thrust faults and normal faults [*Zhang et al.*, 2004]. The current results show that the presence of a bend in a dip-slip fault can also have important consequences for the nucleation process, including significant effects on earthquake nucleation location and timing. A steeper lower fault segment will lead to a shallower earthquake on thrust faults, while earthquakes almost nucleate at the same depth for normal faults with bend angles more positive than −15°. The hypocenter locations on normal faults will shift downward dramatically if the bend angle becomes smaller than −15°, with earthquake nucleation shifting to the lower fault segment. The occurrence time of earthquakes is also strongly affected by a large bend on both thrust and normal faults, implying potentially larger earthquakes could occur on faults with large discontinuities in geometry. This study suggests that a bend of the fault plane, which is common in natural faults, is an important factor for the nucleation process, and it cannot be omitted for realistic earthquake studies. However, it is important to note that the basic qualitative effects of the non-vertical geometry remain in the presence of a bent fault: normal faults are still unclamped at the surface, while thrust faults are still clamped at the surface; the effects of this factor on earthquake nucleation persist.

One possible caveat of our results is that in order to make a comparison between thrust and normal faults, we have assumed the same fault geometry and loading characteristics for both types of faults. In nature, fault geometry and loading for normal

and thrust faults may be substantially different, leading to even more contrasts in the nucleation behavior of these faults. Understanding the complexity of earthquakes in natural faults will require additional studies with more realistic fault geometry and more realistic (i.e., rate-and-state) frictional properties. Another important issue to explore is to include the effects of the dynamic rupture process and multiple earthquake cycles, so that the pre-stress field will be a realistic result of both fault geometry and previous earthquakes on the fault system.

Chapter 4

Earthquake Nucleation on Two Parallel Strike-Slip Faults

4.1 Introduction

Laboratory studies [*Dieterich*, 1978; *Okubo and Dieterich*, 1984; *Ohnaka*, 1996; *Shen and Ohnaka*, 1999] show that earthquake process starts with a extremely slow slip phase that is followed by a phase of rapid self-driven acceleration, and the subsequent onset of unstable rupture propagation over a much wider area. Numerical simulations using the rate- and state- dependent friction law [*Dieterich*, 1979, 1981; *Ruina*, 1983] have also shown that unstable fault slip (earthquake) is initiated from a highly localized patch within which slip spontaneously accelerates by several orders of magnitude within a short time window [*Dieterich*, 1992; *Rice*, 1993; *Lapusta and Rice*, 2002; *Rubin and Ampuero*, 2005; *Ampuero and Rubin*, 2008; *Fang et al.*, 2009a]. The events and interactions of fault slip that lead to the initiation of unstable slip are collectively defined as earthquake nucleation [*Dieterich*, 1987, 1992]

Earthquake nucleation, which determines the time and place of earthquake rupture initiation, is of central importance for understanding a variety of earthquake related phenomena such as foreshocks and aftershocks, triggering effects by tidal stresses and

seismic waves, earthquake interactions, and scaling of premonitory processes. In addition, earthquake nucleation sets initial conditions of the earthquake source, may have a strong effect on the subsequent rupture propagation and strong ground motion.

Because of the importance of earthquake nucleation, a number of numerical studies of earthquake nucleation have been carried out over the last two decades. For numerical and conceptual simplicity, most models of earthquake nucleation focus on faults with a single planar fault plane under pure shear loading conditions [*Tse and Rice*, 1986; *Okubo*, 1989; *Dieterich*, 1992; *Rice*, 1993; *Ben-Zion and Rice*, 1997; *Ampuero et al.*, 2002; *Lapusta and Rice*, 2002; *Shibazaki*, 2002; *Uenishi and Rice*, 2003; *Rubin and Ampuero*, 2005; *Ampuero and Rubin*, 2008; *Fang et al.*, 2009a]. Generally, these studies suggest that earthquake nucleation is a time dependent frictional process that happens within a highly localized patch (nucleation zone) whose size is generally comparable to a scale length L_b [*Dieterich*, 1992; *Rice*, 1993; *Rubin and Ampuero*, 2005; *Fang et al.*, 2009a]. The location of the nucleation patch is usually associated with the transition between stick-slip and steady sliding but is also strongly affected by the stress heterogeneities left by previous events [*Tse and Rice*, 1986, *Rice*, 1993; *Lapusta and Rice*, 2002, *Shibazaki*, 2002]. However, the simplified fault geometry and loading conditions assume constant normal stress throughout the entire nucleation process which is not likely to happen in realistic nucleation processes.

Based on a single spring-slider model under inclined remote loading conditions, *Dieterich and Linker* [1992] demonstrated that normal stress variations have a strong

effect on earthquake nucleation: a decrease in normal stress reduces fault effective stiffness which will destabilize fault slip and advance earthquake nucleation. Based on a 2D plane strain model with shear and normal combined loading, *Fang et al.* [2009b] showed that both nucleation time and nucleation zone dimension are strongly dependent on varying normal stress. Generally, an increase in normal stressing rate will result in a longer nucleation time and a larger nucleation zone while a decrease in normal stressing rate has a reverse effect. Nevertheless, these studies still employ idealized planar fault models in which fault slip will not induce normal stress variations. In nature, faults are usually non-planar, bearing bends, branches and offsets [*Wesnousky*, 1988; *Zachariasen* and *Sieh*, 1995; *Zoback et al*, 1999; *Zampier et al*, 2003; *Brankman* and *Aydin*, 2004]. Inter-seismic slow slip on non-planar fault can cause highly localized stress variations (both shear and normal stress) at the geometric irregularities. In addition, on non-planar faults, fast slip within the nucleation patch not only can induce shear stress concentrations at the edges of the nucleation zone but also may induce large normal stress concentrations locally. Therefore, unlike stress profiles in planar fault models with pure shear or inclined remote stressing which are generally homogeneous along the faults, stress variations on non-planar faults can be extremely heterogeneous and evolve with time. The time dependent heterogeneous stress distribution may exhibit complex effects on nucleation processes, which may gives different characteristics of earthquake nucleation from those observed in simplified fault models.

Few studies have focused on the role of fault geometry in nucleation processes. *Nielsen and Knopoff* [1998] studied the effect of repeated quasi-static ruptures on a non-

planar fault system with extensional and compressional bends. They found that extensional bends were common places for earthquake nucleation, as expected from the reduced yield stress at these locations. *Zhang et al.* [2004, 2006] studied the effect of non-vertical dip-slip fault geometry on rupture nucleation. They suggested that given identical fault geometry (with exception of the direction of tectonic loading), unstable fault slip tend to occur earlier and at shallower depth on thrust faults. However, no study has simulated earthquake nucleation on faults with step-over geometry, which is commonly seen on natural strike-slip faults [e.g. *Wesnousky*, 1988; *Knuepfer*, 1989].

The only study that is related to nucleation on faults with step-over geometry is *Segall and Pollard* [1980] in which they carefully analyzed the static interaction of step-overs. They found that for compressional step-overs, normal stress increases on the overlapped portion of the faults which inhibits frictional sliding, whereas for extensional step-overs, normal stress decreases which facilitates fault slip. Their analysis of stress distributions around step-overs suggest that earthquake swarms and aftershocks cluster may usually happen near extensional step-overs, while compressional step-overs may be sites of large earthquakes. Their results demonstrated the importance of fault interactions and provide us a general picture of stress distributions along faults with step-overs.

Step-overs are shown to have a large effect on the dynamics of earthquake rupture and slip. *Harris et al.* [1991] and *Harris and Day* [1993] used a 2D finite difference algorithm to explore dynamic interactions of two parallel strike-slip faults with homogeneous initial conditions. They found that earthquake rupture can jump both

compressional and extensional step-overs with extensional step-overs allow wider rupture jumps. Their results indicate that an earthquake is unlikely to jump a step-over wider than 5 km. *Duan and Oglesby* [2006] used a 2D finite element model to explore the dynamics of two parallel strike-slip faults over multiple earthquake cycles. They suggested that rupture can jump a 4 km wide compressional step-over and an 8 km or wider extensional step-over if the fault system has historically experienced many earthquakes. A young step-over with less stress heterogeneity only allows rupture to jump smaller step-over widths. The rupture dynamics studies on strike-slip faults with step-overs provide us important criteria about the conditions for rupture jumps across the step-overs. However, like most dynamic rupture models, these studies have uncertainties in rupture nucleation (nucleation location and/or size of the nucleation patch), which may result in different rupture behaviors. To provide more accurate nucleation information and characterizing nucleation process on geometric complex faults, we have carried out a detailed study of nucleation on faults with step-over geometry. In particular, we focused on exploring how step-over affects three important physical aspects of earthquakes: the nucleation time, nucleation locations and nucleation zone dimensions.

4.2 Method

We extended the 2D boundary element method used by *Dieterich* [1992] to simulate nucleation processes with varying normal stress. Faults are assumed to be finite cracks imbedded in an infinite elastic medium and are discretized into n equally spaced segments. A remote stressing is applied to ensure nucleation. For simplicity, the stressing

is assumed to be pure shear and has a constant rate $\dot{\tau}$, which suggest that normal stress variations can only arise from the interactions of step-overs. Faults are then discretized into *n* equally spaced segments. Slip on each fault segment is assumed constant so that there are displacement discontinuities at the edges of every segment which is equivalent to edge dislocations. Stress of each segment is evaluated at the center of the segment. At certain time *t*, stress at element *i* is given by

$$\begin{cases} \tau_i = \tau_i^0 + \dot{\tau}_i t + \Delta\tau_i \\ \sigma_i = \sigma_i^0 + \Delta\sigma_i \end{cases} \tag{4-1}$$

where τ_i, σ_i stands for current shear and normal stress respectively. τ_i^0 and σ_i^0 are the initial stresses and $\dot{\tau}_i$ is the constant pure shear stressing rate. $\Delta\tau_i$ and $\Delta\sigma_i$ are the sum of stress changes resulting from all the dislocations at segment boundaries, which can be calculated as

$$\Delta\tau_i = s_{ij}\delta_j;\ \Delta\sigma_i = n_{ij}\delta_j \tag{4-2}$$

where δ_j is the slip of element *j*. The *n* by *n* interaction coefficients s_{ij} and n_{ij} can be readily calculated from dislocation solutions in an infinite elastic medium.

The shear stress τ is balanced by friction between the fault surfaces. We employ the laboratory derived rate- and state- dependent friction [*Dieterich*, 1979, 1981; *Ruina,* 1983] which is given as

$$\mu = \mu_0 + a \ln \frac{v}{v^*} + b \ln \frac{\theta v^*}{D_C} \tag{4-3}$$

where μ_0 is the friction coefficient when current slip rate v equals v^*, the reference slip rate. θ is the state variable and D_c is the characteristic sliding distance. Parameters a and b are positive and on the order of 10^{-2}. a characterizes the magnitude of the 'direct effect', the increase in friction with increasing slip rate and b characterizes the magnitude of the 'evolution effect', the increase in friction with increasing contact time.

The evolution of the state variable, which empirically represents the evolution of contact populations between the sliding fault interfaces, is found to be dependent on the time elapsed, slip rate and normal stress variations [*Linker and Dieterich*, 1992]

$$\frac{d\theta}{dt} = 1 - \frac{\theta v}{D_c} - \frac{\alpha \theta \dot{\sigma}}{b\sigma} \tag{4-4}$$

The first term '1' on the right represents the strengthening by time of stationary contact observed in laboratory experiments [*Dieterich*, 1972; *Beeler et al*., 1994; *Dieterich and Kilgore*, 1994; *Marone*, 1998]. The second term $\theta v/D_c$ represents the weakening rate of the state variable due to fault slip and is denoted by Ω in the discussion of how it influences nucleation zone size [*Rubin and Ampuero*, 2005; *Fang et al.*, 2009a]. The third term $\Omega_n = \alpha \theta \dot{\sigma} / b\sigma$ represents weakening or healing of a fault from normal stress variations in which α is a constant and has measured values in the range of $0.25 \leq \alpha \leq 0.5$.

4.3 Model Configuration

We carried out analysis on idealized fault model consisting two parallel strike-slip faults imbedded in an infinite elastic medium as shown by Figure 4-1. The two faults are assumed identical and having a length L. Without losing generality, the faults are assumed right lateral and under pure shear remote stressing rate $\dot{\tau} = 1 \times 10^{-3}$ Pa/s. For right lateral fault systems, a left step-over is compressional while a right step-over is extensional. The step-over is mainly controlled by two parameters, the overlapping length d and the offset h. d is allowed to vary from $0.05L$ to $0.95L$, which corresponds to almost no overlap to full overlap. h varies in the range from $5 \times 10^{-4}L$ to $0.15L$. The overlapping end is the location on each fault that coincides with the end of the companion fault when the offset is zero. Nucleation location is defined as the center of the nucleation zone and is specified by two parameters: the along fault distance r, which gives the absolute location of nucleation and the distance to the overlapping end δ, which describes the relative location of nucleation to the overlapping ends.

The generalized shear modulus for plane strain condtions is chosen as G = 40GPa for plane strain conditions and Poisson's ratio is given as 0.25. The initial normal stress σ_0 is set as 100MPa. We use a representative value of b = 0.01 and a = 0.0085 based on laboratory studies of granite [*Linker and Dieterich*, 1992; *Marone*, 1998; *Tullis and Weeks*; 1986]. Poisson's ratio set to be 0.25. The suggested scale length for nucleation size depends on current normal stress σ as $L_b = GD_c/b\sigma$ [*Dieterich*, 1992], which keeps changing if σ is non-constant. Since $\Delta\sigma$ is usually small compared to σ_0, for comparison

purposes, we choose $\sigma = \sigma_0$ which yields $L_b = GD_c/b\sigma_0 = 40{,}000D_c$. Nucleation size is found to be dependent on fault length [*Fang et al.*, 2009a]. To compare nucleation sizes on faults with step-overs with those on single planar faults given in *Fang et al.*, [2009a], we still choose the same fault length as $1.2\times10^7 D_c$ in length which equals $300L_b$.

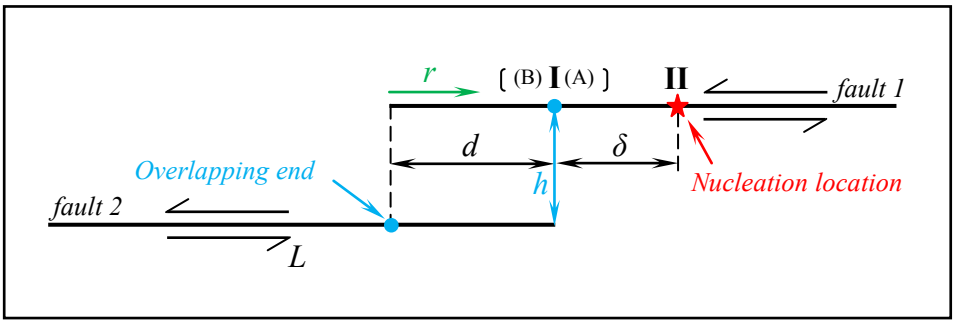

Figure 4-1. A schematic illustration of the model of two parallel faults with a step-over. The two faults are identical with length L. The dots represent overlapping ends while the star represents nucleation location. The step-over geometry is controlled by two parameters, the overlapping length d and the offset h. Nucleation location is described in by two parameters: the along fault distance r and the distance δ to the overlapping end on the same fault.

In our study, we assume homogeneous initial conditions to isolate the effect of step-over on earthquake nucleation. We are fully aware that the initial conditions must be heterogeneous to some extent as suggested by *Duan and Oglesby* [2006] that fault heterogeneity increases with the numbers of earthquake cycles experienced. For completeness, we also investigate the general effect of heterogeneous initial conditions

based on simulations results using random initial conditions. A more complete study of earthquake nucleation on two parallel faults with heterogeneous initial conditions requires systematic quantification of fault heterogeneity, which is beyond the scope of this study.

4.4 Results

First, we focused on characterizing how nucleation is affected by the offset of the two parallel faults with fixed overlapping length. Three representative overlapping situations have been studied with overlapping length chosen as d/L = 0.1, 0.5 and 0.9, which corresponds to nearly no overlapping, half overlapping and almost fully overlapping. All simulations start with homogeneous initial conditions as $v_0/D_c = 0.1\text{s}^{-1}$ and θ_0 = 1s (Ω_0 = 0.1), which is a general representation of conditions right after a previous earthquake. Our simulation results show that there is only a small variation of nucleation time (less than 1%) for all the cases studied which is broadly consistent with the results shown by *Fang et al.*, [2009b] that nucleation time is mainly controlled by initial conditions (v_0/D_c, θ_0) if the fault is initially sliding below steady state ($\Omega_0 < 1$). However, unlike nucleation time, both nucleation location and nucleation size are found to be strongly affected by fault geometry and are illustrated in detail in Figure 4-2.

As shown by Figure 4-2(a-c), nucleation location varies with overlapping length d and offset h in a rather complex way for both compressional and extensional step-overs. When overlapping length is small as $d = 0.1L$ (Figure 1a), nucleate location varies with

offset in the same way for both compressional and extensional step-overs. In particular, earthquake always nucleates in the vicinity of the overlapping end (outside of the overlapping zone) when h is smaller than $0.01L$. As h gets larger than $0.01L$, nucleation location progressively migrates further away from the overlapping end and toward the fault center. The trend of nucleation migration in this case is relatively easy to interpret. When the offset is small, the step-over causes strong stress variations around the overlapping ends, which are locations of nucleation. As offset becomes larger, the effect of the step-over progressively diminished and nucleation location becomes closer to fault center which is always the location for nucleation if the companion fault does not exist. One may also notice that nucleation never occurs within the overlapping region.

When overlapping length is $d = 0.5L$ (Figure 4-2b), nucleation location varies in quite different ways for the two different step-overs. For compressinal step-overs, earthquakes still nucleate further away from the overlapping zone as offset increases. However, for extensional step-overs, nucleation location migrates toward the overlapping zone and for offsets larger than $0.025L$, nucleation can actually occur slightly within the overlapping zone.

When overlapping length is large as $d = 0.9L$ (Figure 4-2c), nucleation location again varies significantly for the two different step-overs. For extensional step-overs, nucleation location varies in the same trend as that of $d = 0.5L$. However, for compressional step-overs, nucleation location is not always outside of the overlapping zone. It shifts deep into the overlapping zone as offset increases from $0.025L$ to $0.05L$.

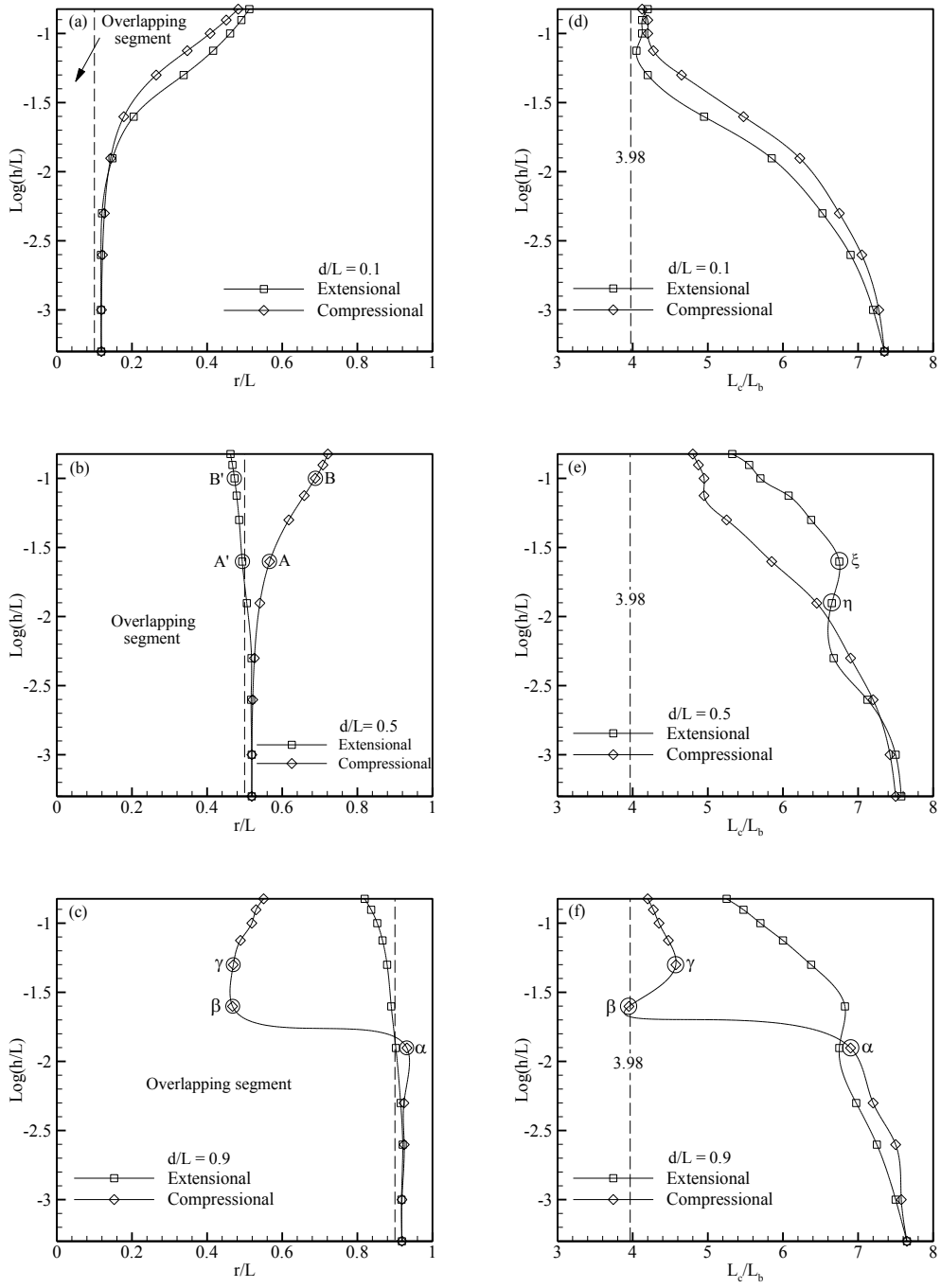

Figure 4-2. Nucleation location (a-c) and nucleation size (d-f) as a function of offset *h* for both extensional and compressional step-overs for three representative overlapping situations (a,d) $d = 0.1L$ (b,e) $d = 0.5L$ and (c,f) $d = 0.9L$.

As shown by Figure 4-2(d-f), nucleation size also changes with overlapping length and offsets in a very complex manner. Nucleation size of a single planar fault (denoted by dashed line) is also shown in Figure 4-2(d-f) for comparison. In general, nucleation size increases as offset decreases and it can becomes almost twice larger than that of a single planar fault when offset is extremely small. However, nucleation size does not always vary smoothly with offset. For example, there is a slight decrease of nucleation size when offset decreases from $0.05L$ to $0.025L$ for extensional step-over with overlapping length $d = 0.5L$ (denoted by ξ and η in Figure 4-2e). Another example is that there is an unusually large decrease of nucleation size when offset changes from $0.075L$ to $0.05L$ for compressional step-over with overlapping length $d = 0.9L$. The severe decrease of nucleation size is is followed by a more severe increase of nucleation size when offset decreases from $0.05L$ to $0.025L$ (denoted by α, β and γ in Figure 4-2f). Compared with Figure 4-2(a-c), the unusual changes of nucleation size seem to correlate with migration of nucleation location into different regions. From Figure 4-2(b) and 4-2(e), change of nucleation size from ξ and η corresponds to migration of nucleation location into the overlapping zone from outside. Similarly, inferred from Figure 4-2(c) and 4-2(f), the abnormal changes of nucleation size from α, to β and γ coincide with significant changes in nucleation location.

The complex pattern of nucleation location migration as the two faults are moved apart (increasing offset) is mainly controlled by changes in elastic stress interactions as the step-over fault geometry changes. When normal stress is non-constant, evolution of

fault slip is found to depend on a modified Coulomb stress ΔS_α [*Dieterich et al.*, 2000; *Fang et al.*, 2009b]

$$\Delta S_\alpha = \Delta\tau - (\mu - \alpha)\Delta\sigma \tag{4-5}$$

where $\Delta\tau$ and $\Delta\sigma$ are changes of shear and normal stress due to fault slip with compression defined positive. Figure 4-3 and Figure 4-4 are plots of sequences of slip rates [Figure 4-3(a,b) and 4-4(a,b)] and changes of the modified Coulomb stress [Figure 4-3(c,d) and Figure 4-4(c,d)]. The sequences of the modified Coulomb stress plotted are those in the very early stage of nucleation in which rapid acceleration and localization of fault slip has not occurred. Comparing sequences of slip rate and the corresponding profiles of the modified Coulomb stress, the locations that correspond to peaks of the modified Coulomb stress turn out to be places that nucleation first develops. Unless the late stage nucleation zone expansion [*Rubin and Ampuero*, 2005; *Fang et al.*, 2009a] is highly asymmetric, these locations eventually will be the center of the expanding nucleation zone and are defined as nucleation locations. From Figure 4-3 and Figure 4-4, it is obvious that nucleation location is determined by the modified Coulomb stress changes in the very early stages of nucleation process.

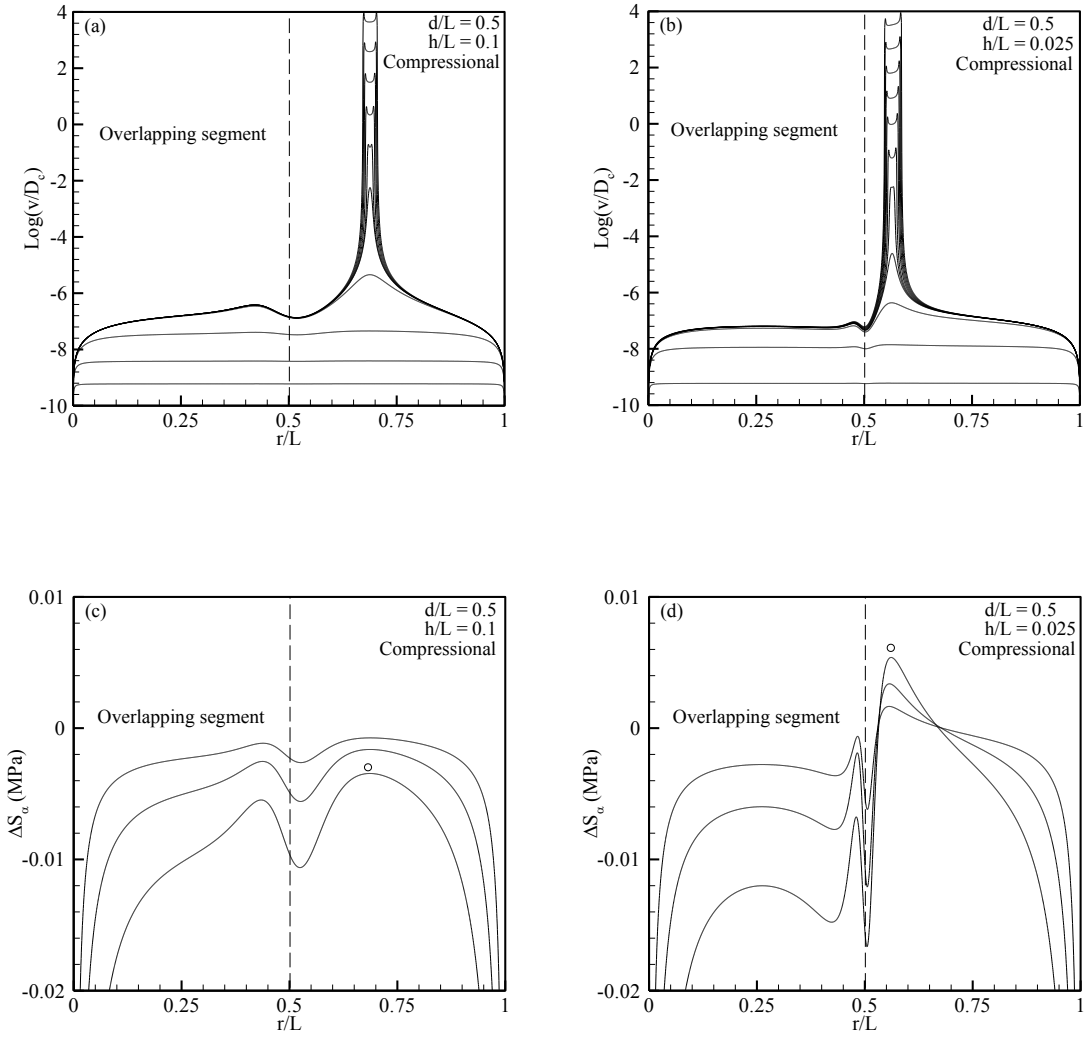

Figure 4-3. Sequences of fault slip rate and Coulomb stress change profiles for point A and B in Figure 4-2(b). In (b,d), only early stage Coulomb stress changes are plotted for illustration. The locations with peaks of Coulomb stress changes are places where fast slip first develops. Unless nucleation zone expansion is highly asymmetric, these locations will be the center of the expanding nucleation zone and correspond to the nucleation location.

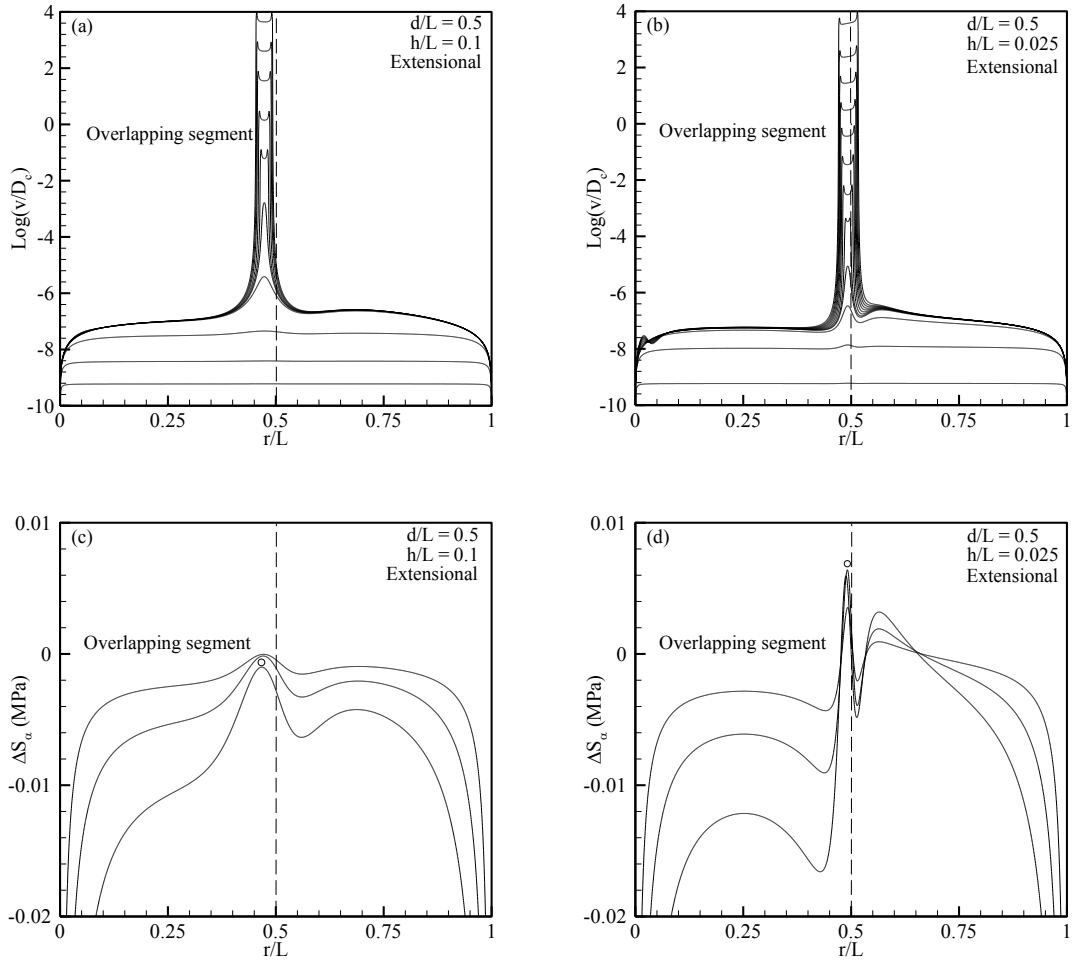

Figure 4-4. Fault slip rate and Coulomb stress change profiles for point A' and B' in Figure 4-2(b). Similarly, nucleation locations seem to be controlled by peaks of Coulomb stress change in the very early stage of nucleation.

The abrupt changes of nucleation size from the general trend occurred at some critical geometric configuration discussed above can be explained by the evolution of the combined variable Ω at the nucleation location. On faults with constant normal stress, it is shown that nucleation zone expansion will not occur unless Ω at the center of the nucleation zone decreases to a critical value Ω_c near 1 at the late stage of nucleation [*Rubin and Ampuero*, 2005; *Fang et al.*, 2009a]. When normal stress is non-constant, *Fang et al.*, [2009b] showed that the third term in equation (4-4) $\alpha\theta\dot{\sigma}/b\sigma$ is negligible in the late stage of nucleation due to significant decrease of the state variable. Therefore, the beginning of nucleation zone expansion should still be marked by decrease of Ω to the critical value Ω_c when normal stress is non-constant.

Figure 4-5 demonstrates the cause of the abrupt changes of nucleation size when the offset changes from $0.025L$ to $0.05L$ with $d = 0.9L$. Figure 4-5(a) and 4-5(b) show the evolution of Ω as a function of slip rate at the nucleation zone center for compressional and extensional step-overs respectively. Results from a single planar fault are also shown for comparison. From Figure 4-5(a), Ω decreases to the critical value Ω_c at a much larger slip rate (about three orders larger) for $h = 0.05L$ as compared to the case with $h = 0.025L$. Ω_c achieved at larger slip rate implies later nucleation zone expansion. It is also shown that the increase of nucleation size for every order increase of slip rate at the nucleation zone center is almost the same [*Fang et al.*, 2009a]. Since nucleation processes are always assumed to end at a fixed critical slip rate v_i, then nucleation zone expansion occurred at larger slip rate will result in a smaller nucleation size. In Figure 4-5(b), Ω reaches Ω_c at a slightly smaller slip rate for $h = 0.05L$ as compared to the case with $h =$

0.025L, which leads to a slight increase of nucleation size. However, one may notice in Figure 4-5(a), for h = 0.05, Ω actually reaches Ω_c at smaller slip rate than that for a single fault. However, the nucleation size for h = 0.05 is smaller which does not agree with the general mechanism that nucleation size should be larger if Ω_c is reached at a smaller slip rate.

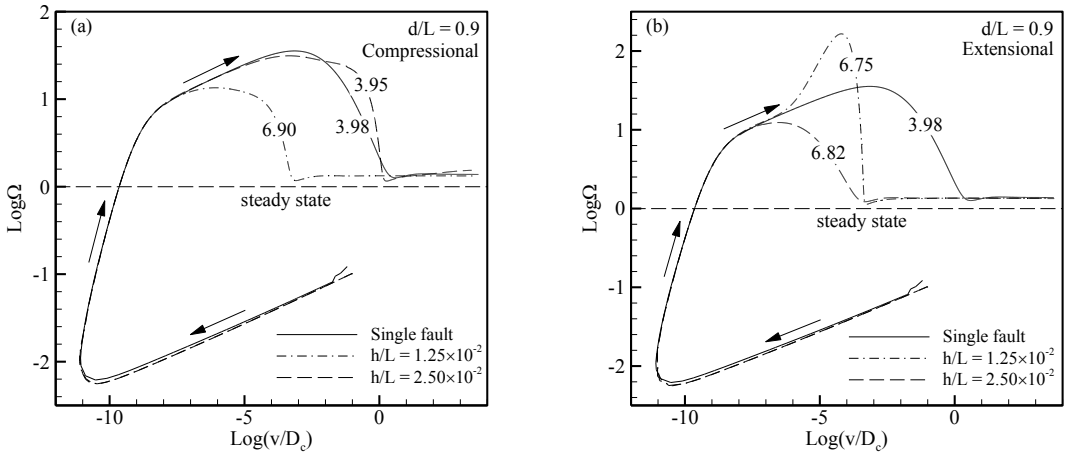

Figure 4-5. Evolution of Ω at the center of the nucleation zone. (a) compressional step-overs, (b) extensional step-overs. Results from a single planar fault are also shown for comparison. The numbers on every curve indicated nucleation size L_c/L_b.

The cause of this abrupt behavior is that nucleation zone expansion for the case with h = 0.05 and d = 0.9L is extremely asymmetric as shown in Figure 4-6(a). When nucleation zone expansion is highly asymmetric, the increase of nucleation size for every order increase of slip rate at the nucleation zone center will be different from that for

symmetric nucleation zone expansion. Therefore, although Ω may reach Ω_c at a smaller slip rate for highly asymmetric nucleation zone, it is not guaranteed that the resulting nucleation size will be larger. Our results suggest that non-symmetric nucleation zone expansion mostly appears when nucleation occurs near the overlapping ends where the variations of normal stress are more significant and highly heterogeneous. An expanding nucleation zone can be viewed as an expanding crack. The advancing crack front will slow down if it enters a zone with increasing normal stress (i.e. the crack front is being clamped) and vice versa. However, for the case shown in Figure 4-6(a), nucleation occurs so far away from the overlapping end that normal stress variations resulting from the step-over geometry must be too small to cause such severe non-symmetric expansion. It turns out that the non-symmetric expansion is controlled by normal stress variations resulted from the fast slipping patch on the companion fault. Figure 4-6(b) shows the sequence of normal stress variations along the fault. It is shown that nucleation on the companion fault induces large normal stress variations which forms two region with one is being clamped and the other is being unclamped. Comparing Figure 4-6(a) and 4-6(b), the nucleation zone edge that is in the zone with decreased normal stress advances much faster than the other edge, results in a highly asymmetric nucleation zone. Figure 4-6 suggest that the interactions of adjacent nucleation zone which always happens at the very late stage of nucleation can also strongly alter nucleation size, which adds more complexity to nucleation on two parallel faults with step-overs.

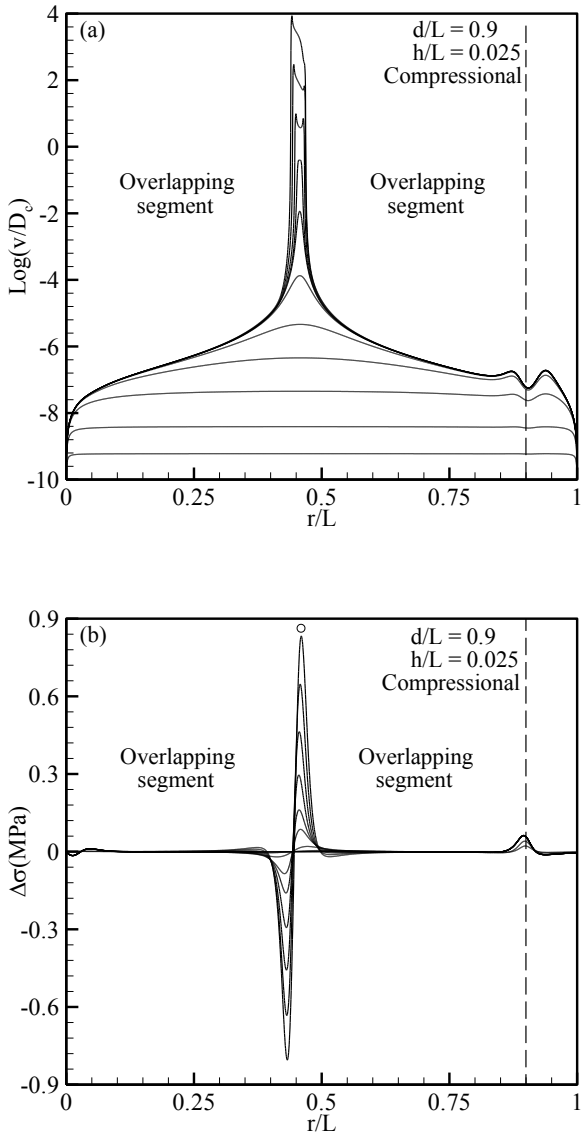

Figure 4-6. (a) Sequences of slip rate for nucleation on a compressional step-over with $d = 0.9L$ and offset $h = 0.025L$. The nucleation zone expansion is highly asymmetric. (b) Sequences of normal stress variations along fault. The large peaks of normal stress variation are induced by the fast slipping nucleation patch on the companion fault.

In order to give a complete picture about how nucleation location and nucleation size change with the geometry of the two parallel faults. A series of simulations have been carried out with the overlapping length d and offset h systematically studied. Figure 4-7(a) and 4-7(b) are contour plots of nucleation location with respect to different d and h. In order to better describe the relationship between nucleation location and the overlapping ends, we choose to quantify nucleation location by δ, which is the distance between nucleation location and the overlapping ends. Furthermore, we divide the fault into two regions which is denoted in Figure 4-1. Region I is the fault segment that is in the very vicinity (within $0.05L$) of the overlapping end while region II spans the rest of the fault. Therefore, if nucleation occurs within region I, then nucleation location is very close to the overlapping end. In addition, region I is further divided into two sub-regions (A) and (B) with (B) encompass the portion of region I that is inside the overlapping zone. In Figure 4-7(a), for faults with compressional step-overs, nucleation generally occurs near the overlapping end outside the overlapping zone [region I(A)] for offset smaller than $0.01L$. For offset larger than $0.01L$, nucleation always occurs far from the overlapping end (in region II). For faults with extensional step-overs shown in Figure 4-7(b), except some extreme overlapping situations, nucleation always occurs near the overlapping end for all offsets studied. When offset is smaller than $0.01L$, nucleation location falls in region I(A) while it migrates to region I(B) for larger offsets.

Based on results from Figure 4-7(a) and 4-7(b), for both kinds of step-overs, earthquakes generally tend to nucleate near the overlapping end but outside the overlapping zone when the offset is smaller than $0.01L$, which is equivalent to $1.2\times10^{5}D_c$

or $3L_b$ in current parameter settings. As discussed by Figure 4-3 and 4-4, nucleation locations generally coincide with the peaks of the modified Coulomb stress at the early stage of nucleation. Therefore, for two parallel faults with offsets smaller than $0.01L$, homogeneous fault slip before slip localization is expected to induce Coulomb stress changes that are peaked at the observed nucleation location. When the offset is larger than $0.01L$, earthquakes still nucleate near the overlapping near the overlapping end for extensional step-overs while they tend to nucleate further away from the overlapping end for compressional step-overs. From Figure 4-7(c) and 4-7(d), nucleation size generally decreases with increasing offsets for both kinds of step-overs.

The distinction of earthquake nucleation locations for the two kinds of step-overs with large offsets can be explained by examining the elastic stress field near the two faults. The elastic stress distributions used for illustration are calculated from cases with $d = 0.5L$ and $h = 0.025L$. As shown by Figure 4-8(a1) and 4-8(b1), the elastic shear stress around both kinds of step-overs are exactly the same. In particular, fault slip generally relaxes shear stress within the overlapping zone ($\Delta\tau < 0$). The only exception is that there are two narrow zones of shear stress increases (marked by small eclipses) that radiate from the two fault ends. Outside the overlapping zone, stress concentration from the fault end (crack tip) sheds a large zone of increasing shear stress on its companion fault (marked by large eclipses). The identical shear stress field around the compressional and extensional step-overs suggests that the difference in the nucleation locations does not result from slip induced shear stress variations. However, as shown by Figure 4-8(a2) and 4-8(b2), the elastic normal stress fields are absolutely reversed for the two different step-

overs. Generally, fault slip raises normal stress inside the overlapping zone for compressional step-overs but reduces normal stress within the overlapping zone for extensional step-overs. The overlapping end is shown to be the location of the peak of normal stress variations. For compressional step-overs, the immediate vicinity of the overlapping end is severely unclamped [marked by the eclipse in Figure 4-8(a2)]. This unclamped zone is bounded by two regions with increasing normal stress which are marked by the two rectangular in Figure 4-8(a2). For extensional step-overs shown in Figure 4-8(b2), the distribution of normal stress around the overlapping ends is reversed. The immediate vicinity of the overlapping end is being severely clamped and the further regions from the both sides are being strongly unclamped. The reversed normal stress distribution, combined with the identical shear stress distribution, results in different distributions of the modified Coulomb stress ΔS_α for the two different step-overs and are shown in Figure 4-8(a3) and 4-8(b3). In Figure 4-8(a3), the modified Coulomb stress peak coincides with the shear stress peak outside the overlap zone shown in Figure 4-8(a1). The shear stress peak inside the overlapping zone does not produce a Coulomb stress peak due to increased normal stress at the location. As a result, nucleation mostly happens outside the overlapping zone unless the two faults are becoming almost fully overlapped. On the contrary, for extensional step-overs, the shear stress peak inside the overlapping zone results in a larger Coulomb stress peak due to decreased normal stress at the location. Therefore, earthquakes tend to nucleate slightly inside the overlapping zone for extensional step-overs having offsets larger than $0.01L$.

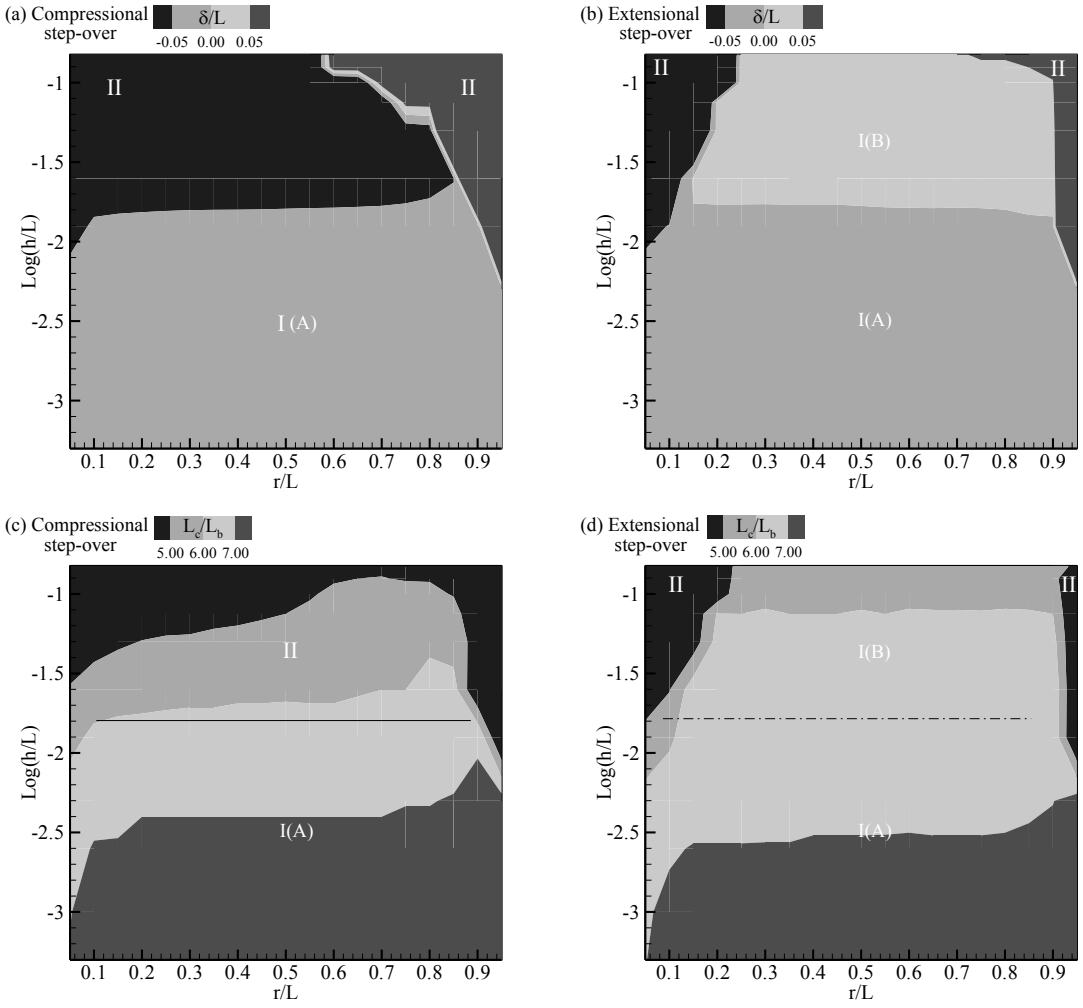

Figure 4-7. Contour plots of (a,b) nucleation location and (c,d) nucleation size as functions of overlapping length *d* and offset *h*. Nucleation location is described by *δ*, the distance between the nucleation location and the overlapping end.

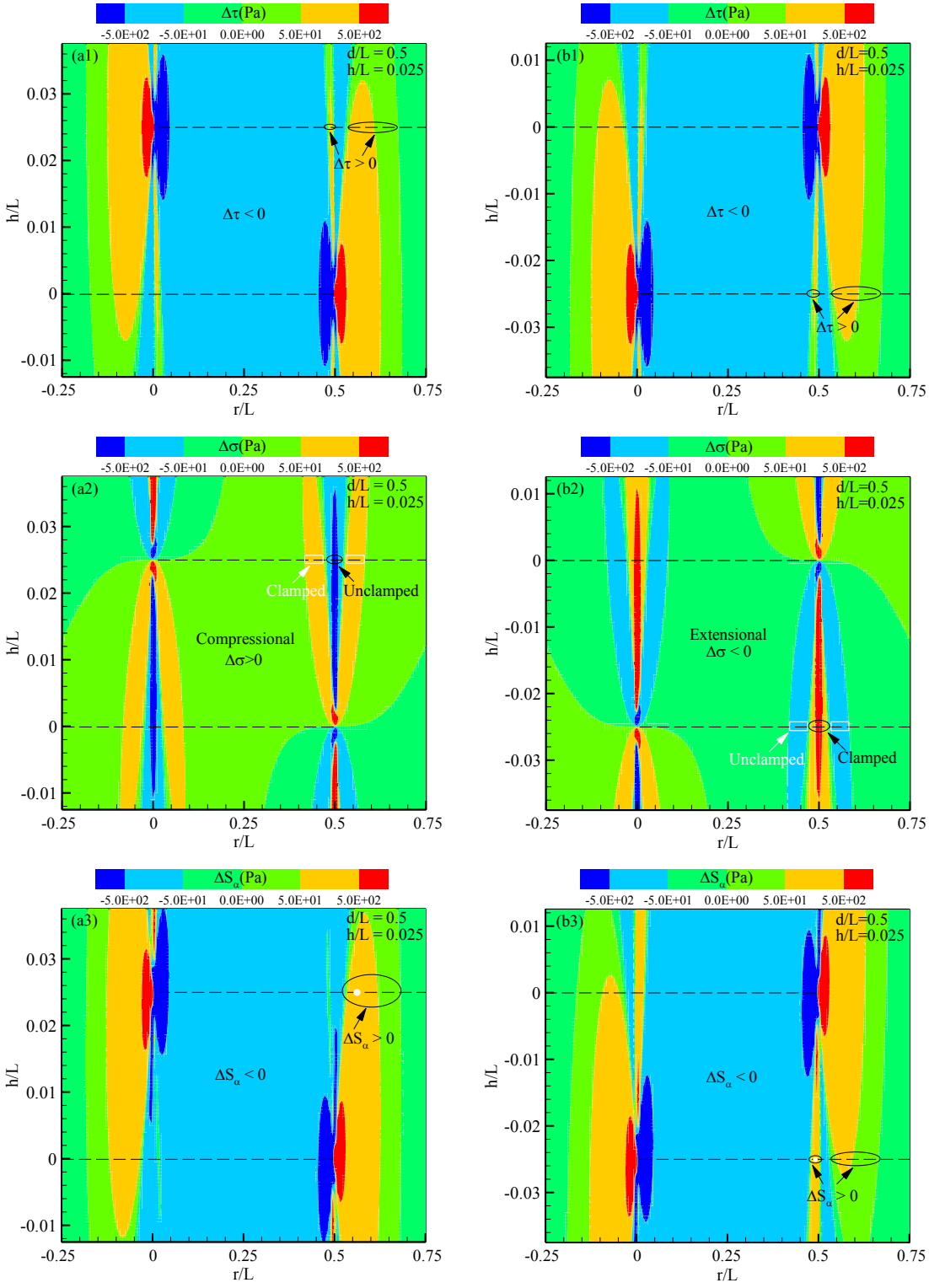
Δτ(Pa)
-5.0E+02 -5.0E+01 0.0E+00 5.0E+01 5.0E+02
(a1)
d/L = 0.5
h/L = 0.025
Δτ > 0
Δτ < 0
h/L
r/L
(b1)
d/L=0.5
h/L=0.025
Δσ(Pa)
(a2)
Clamped
Unclamped
Compressional
Δσ>0
(b2)
Extensional
Δσ < 0
ΔS$_\alpha$(Pa)
(a3)
ΔS$_\alpha$ > 0
ΔS$_\alpha$ < 0
(b3)

Figure 4-8. Change of stress due to fault slip around compressional (a1-a3) and extensional (b1-b3) step-overs. From (a1) and (b1), the changes of shear stress are the same for both kinds of step-overs. However, from (a2) and (b2), the changes of normal stress are reversed. The resulting modified Coulomb stress change shown in (a3) and (b3) is slightly different for the two kinds of step-overs.

4.5 Discussion and Conclusions

1. The effect of heterogeneous initial condition

All the results listed above are from simulations started from homogeneous initial conditions. As discussed in the introduction section, earthquake nucleation processes occurring on natural faults are expected to have heterogeneous initial conditions. To fully explore the effect of heterogeneous initial conditions on earthquake nucleation requires systematic quantification of fault heterogeneity and is beyond the scope of this paper. We have investigated the general effects of heterogeneous initial conditions on earthquake nucleation by applying random initial conditions to faults.

Figure 4-9(a1-b2) are plots of sequences of slip rate profiles from two half overlapping parallel faults with offsets equal to $0.025L$ and $0.05L$. (a1) and (b1) shows nucleation from homogeneous initial conditions while (a2) and (b2) shows nucleation from heterogeneous initial conditions with the same fault geometry. Comparing the results suggests that heterogeneous initial condition competes with the step-over geometry in determining the location of earthquake nucleation. When the offset is small

(0.025L), the effect of fault geometry is more prominent. Nucleation location is determined by the step-over geometry and there is no difference in the location of nucleation for homogeneous or heterogeneous initial conditions. When the offset is large (0.05L), the effect of heterogeneous initial conditions becomes dominant and nucleation location always corresponds to locations with highest initial slip rate. Based on equation (4-3), the initial friction on the fault can be expressed as

$$\mu = \mu_0 + (1 - \ln \Omega) \ln \frac{v}{v^*} \tag{4-6}$$

With Ω assumed homogeneous along fault, the location with highest initial slip rate actually is the place with highest initial friction. The critical offset at which the effect of fault geometry is overwhelmed by the effect of heterogeneous initial conditions is not unique and is strongly affected by the severity of fault heterogeneity which is still uncertain for natural faults before we can systematically quantify three dimensional fault heterogeneities. This uncertainty in fault heterogeneity makes nucleation on natural faults with complex geometry more complicated and prohibits us from making reliable predictions in nucleation locations.

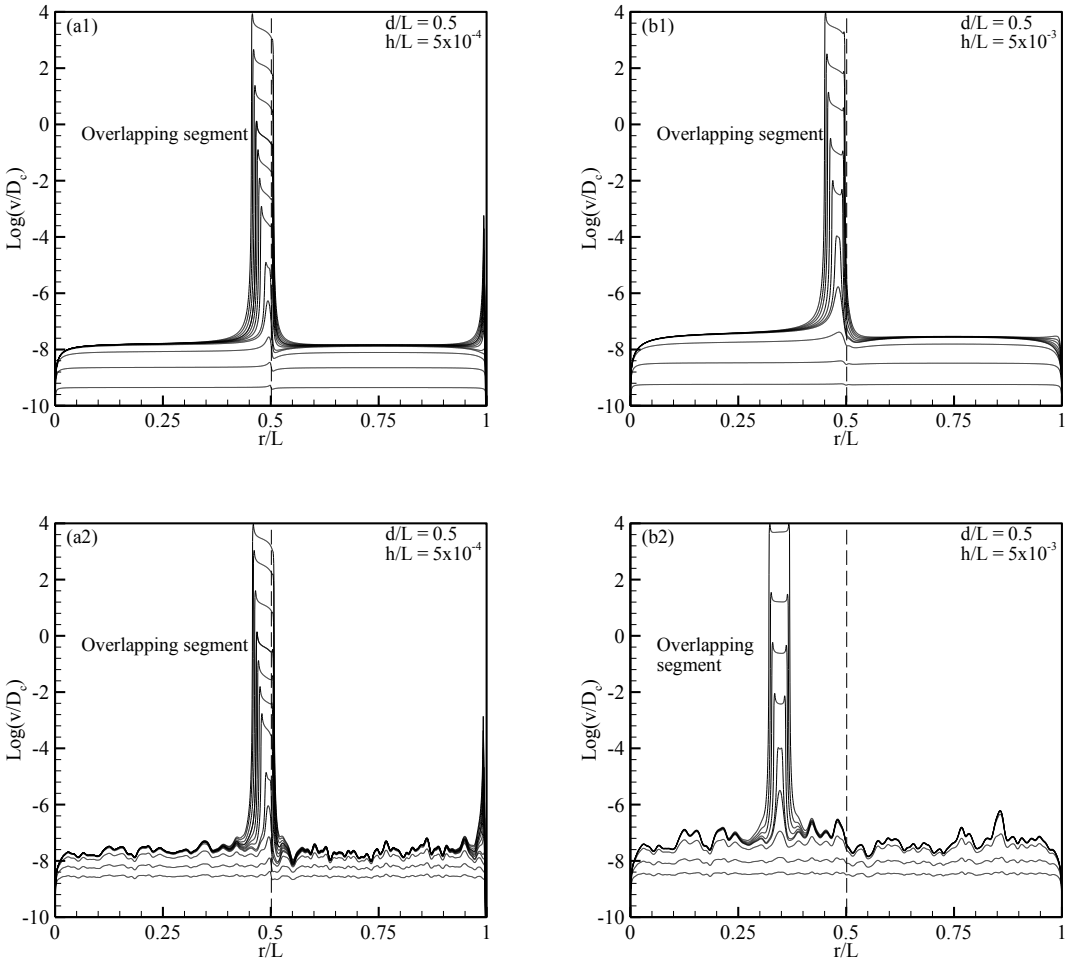

Figure 4-9. Sequences of slip rate along fault during the nucleation processes. (a1, b1) simulations start from homogeneous initial conditions, (a2, b2) simulations start from heterogeneous initial conditions. Earthquakes tend to nucleate at the location with the largest initial friction unless the offset is small enough.

2. The implications to jumping of earthquake rupture

Natural earthquakes occurred on segmented faults with step-overs have been observed to jump from one segment to the next. For example, the 1992 Landers earthquake jumped across several geometrical boundaries to rupture at least five fault segments [*Sieh et al.*, 1993]. The 1999 Izmit, Turkey, earthquake also broke four distinct segments of the North Anatolian fault, [*Lettis et al.*, 2002]. The understanding of conditions that control jump of earthquake rupture across fault offsets onto neighboring segments and cascade into a much larger earthquake is of crucial importance in seismic hazard analysis. Systematic numerical studies suggest that earthquake rupture can jump more easily across an extensional step-over than a compressional step-over because of the difference in transient stress field generated by the two kinds of step-over features [*Harris et al.*, 1991; *Harris and Day*, 1993; 1999; *Duan and Oglesby*, 2006]. Based on our results, earthquakes can probably jump wider gaps between the fault segments than those suggested by these rupture dynamics studies if the time dependent nucleation process is included. The reason for this conjecture is elaborated in the following. Earthquake nucleation can proceed simultaneously on different fault segments. With heterogeneous sliding conditions, one segment may reach instability earlier than others. The resulting earthquake rupture propagates outward. When earthquake rupture propagates into the overlapping zone and becomes closer to the fault end, it exerts significant transient stress loadings to the adjacent fault. If the nucleation patch on the adjacent fault happens to be in the final stage of nucleation, a very small transient stress loading from the earthquake rupture would be sufficient pushes fault slip to instability

instantaneously and the earthquake then cascads into a larger one. Based on the rate- and state- friction formulations, the amount of stress increase needed to push the nucleating patch to instability can be quite small and depends on the slip rate of the patch at the time of the transient stress step. The distance between the two parallel faults required to generate such transient stress step may be larger than that needed to generate a large enough transient stress step to help rupture jump to the next segment without triggering a second earthquake.

Our study on earthquake nucleation on two parallel faults with step-overs suggests that the step-over geometry has a large effect on nucleation location and nucleation size. In particular, when two faults are close to each other (smaller than $0.01L$ based on our parameter settings), earthquakes tend to occur near the overlapping ends for both kinds of step-overs. As the two faults become further apart, for compressional step-overs, earthquake location gradually migrates away from overlapping end and toward the fault center. For extensional step-overs, nucleation still occurs near the overlapping ends but inside the overlapping zone. When heterogeneous initial conditions are considered, the effect of fault geometry on earthquake nucleation can only be observed when the offset is small. Our results also imply that earthquake rupture may jump across the step-over by triggering a second earthquake on the next segment, which may occur on parallel faults with offsets larger than those suggested by rupture dynamics studies without considering triggering of a nucleating earthquake on the adjacent fault. A future study on multiple earthquake cycles on two parallel faults with complete quasi-static modeling of

earthquake nucleation and dynamic modeling of earthquake rupture propagations would reveal more information about the possibility of jumping ruptures.

References:

[1] Aagaard, B. T., T. H. Heaton, and J. F. Hall, Dynamic earthquake ruptures in the presence of lithostatic normal stresses: Implications for friction models and heat production, *Bull. Seismol. Soc. Am.*, *91*, 1765-1796, 2001.

[2] Ampuero, J. P., J. P. Vilotte, and F. J. Sa´nchez-Sezma, Nucleation of rupture under slip-dependent friction law: Simple models of fault zone, *J. Geophys. Res.*, *107*, 2324, doi:10.1029/2001JB000452, 2002.

[3] Ampuero, J. P. and A. M. Rubin, Earthquake nucleation on rate- and state- faults - aging and slip laws, *J. Geophys. Res.*, *113*, B01302, doi: 10.1029/2007JB005082, 2008.

[4] Andrews, D. J., Rupture propagation with finite stress in antiplane strain, *J. Geophys. Res*., *81*, 3575-3582, 1976a.

[5] Andrews, D. J., Rupture velocity of plane strain shear cracks, *J. Geophys. Res.*, *81*, 5679-5687, 1976b.

[6] Baumberger, T., Contact dynamics and friction at a solid-solid interface: material versus statistical aspects, *Solid State Commun.*, *102*, 175-185, 1997.

[7] Baumberger, T. and P. Berthoud, Physical analysis of the state- and rate- dependent friction law II: dynamic friction, *Phys. Rev. B*, *60*, 3928-3939, 1999.

[8] Beeler, N. M., T. E. Tullis, and J. D. Weeks, The roles of time and displacement in the evolution effect in rock friction, *Geophys. Res. Lett.*, *21*, 1987-1990, 1994.

[9] Beeler, N. M, Tullis, T. E., Blanpied, M. L., and Weeks, J. D., Frictional behavior of large displacement experimental faults, *J. Geophys. Res.*, *101*, 8697-8715, 1996

[10] Ben-Zion, Y., and J. R. Rice, Dynamic simulations of slip on a smooth fault in an elastic solid, *J. Geophys. Res*., *102*, 17,771-17,784, 1997.

[11] Berthoud, P. and T. Baumberger, Physical analysis of the state- and rate- dependent friction law: static friction, *Phys. Rev. B*, *59*, 14,313-14,325, 1999.

[12] Biegel, R. L., C. G. Sammis, and J. H. Dieterich, The frictional properties of a simulated gouge having a fractal particle distribution, *J. Struct. Geol.*, *11*, 827-846, 1989.

[13] Blanpied, M. L., and T. E. Tullis, The stability and behavior of a frictional system with a two state variable constitutive law, *Pure Appl. Geophys.*, *124*, 415-444, 1986.

[14] Blanpied, M. L., D. A. Locknet, and J. D. Byeflee, Fault stability inferred from granite sliding experiments at hydrothermal condition. *Geophys. Res. Lett.*, *18*, 609-612, 1991.

[15] Blanpied, M. L., D. A. Locknet, and J. D. Byeflee, Frictional slip of granite at hydrothermal condition. *J. Geophys. Res.*, *100*, 13,045-13,064, 1995.

[16] Blanpied, M. L., T. E. Tullis, and J. D. Weeks, Effects of slip, slip rate, and shear heating on the friction of granite, *J. Geophys. Res.*, *103*, 489-511, 1998a.

[17] Blanpied, M. L., C. J. Marone, D. A. Lockner, J. D. Byerlee, and D. P. King, Quantitative measure of the variation in fault rheology due to fluid-rock interactions, *J. Geophys. Res.*, 103, 9691-9712, 1998b.

[18] Brankman, C. M., and A. Aydin, Uplift and contractional deformation along a segmented strike-slip fault system: the Gargano Promontory, southern Italy, *J. Struct. Geol.*, *26*, 807-824, 2004.

[19] Brechet, Y., and Y. Estrin, The effect of strain rate sensitivity on dynamic friction of metals, *Scri. Metall. Mater.*, *30*, 1449-1454, 1994.

[20] Brune, J. N., Particle motions in a physical model of shallow angle thrust faulting, *Proc. Indian Acad, Sci. Earth Planet. Sci.*, *105*, 197-206, 1996.

[21] Brune, J. N., and A. Anooshehpoor, Dynamic geometrical effects on strong ground motion in a normal fault, *J. Geophys. Res.*, *104*, 809– 851, 1999.

[22] Bouchon, M. and D. Streiff, Propagation of a shear crack on a non-planar fault: a method of calculation, *Bull. Seismol. Soc. Am.*, *81*, 61-66, 1997

[23] Chester, F. M., Effects of temperature on friction: Constitutive equations and experiments with fault gouge, *J. Geophys. Res.*, *99*, 7247-7261, 1994.

[24] Chinnery, M., The stress changes that accompany strike-slip faulting, *Bull. Seismol. Soc. Am.*, *53*, 921–932, 1963.

[25] Cochard, A. and R. Madaraiga, Complexity of slip due to highly rate dependent friction, *J. Geophys. Res.*, *101*, 25,363-25,336, 1996.

[26] Day, S. M., Three-dimensional simulation of spontaneous rupture: the effect of nonuniform prestress, *Bull. Seismol. Soc. Am.*, *72*, 1881-1902, 1982.

[27] Dieterich, J. H., Time-dependent friction in rocks, *J. Geophys. Res.*, *77*, 3690-3697, 1972.

[28] Dieterich, J. H., Preseismic fault slip and earthquake prediction, *J. Geophys. Res.*, *83*, 3940-3948, 1978

[29] Dieterich, J. H., Modeling of rock friction, 1, Experimental results and constitutive equations, *J. Geophys. Res.*, *84*, 2161-2168, 1979.

[30] Dieterich, J. H., Constitutive Properties of faults with simulated gouge, *Mechanical Behavior of Crustal Rocks*, *Geophysical Monograph 24*, Am. Geophys. Union, Washington, DC, pp. 103-120, 1981.

[31] Dieterich, J. H., and G. Conrad, Effect of humidity on time- and velocity-dependent friction in rocks, *J. Geophys. Res.*, *89*, 4196-4202, 1984.

[32] Dieterich, J. H., A model for the nucleation of earthquake slip, *Geophysical Monograph*, *37*, 37-47, 1986.

[33] Dieterich, J. H., Earthquake nucleation on faults with rate- and state- dependent strength. *Tectonophysics*, *211*, 115-134, 1992.

[34] Dieterich, J. H., A constitutive law for rate of earthquake production and its application to earthquake clustering, *J. Geophys. Res.*, *99*, 2061-2618, 1994.

[35] Dieterich, J. H. and B. D. Kilgore, Direct observation of frictional contacts: New insights for state-dependent properties, *Pure Appl. Geophys.*, *143*, 283- 302, 1994.

[36] Dieterich, J. H. and B. D. Kilgore, Imaging surface contacts: Power law contact distributions and contact stresses in quartz, calcite, glass and acrylic plastic, *Tectonophysics*, *256*, 219-239, 1996.

[37] Dieterich, J. H., V. Cayol, P. Okubo, The use of earthquake rate changes as a stress meter at Kilauea volcano, *Nature* , *408* , 457-460, 2000.

[38] Duan, B. and D. D. Oglesby, Multicycle dynamics of nonplanar strike-slip faults, *J. Geophys. Res.*, *110*, B03304, doi:10.1029/2004JB003298, 2005.

[39] Duan, B., and D. D. Oglesby, Nonuniform prestress from prior earthquakesand the effect on dynamics of branched fault systems, *J. Geophys. Res.*, *112*, B05308, doi:10.1029/2006JB004443, 2007.

[40] Dunham, E. M., P. Favreau, and J. M. Carlson, A supershear transition mechanism for cracks, *Science*, *299*, 1557-1559, 2003.

[41] Fang, Z., J. H. Dieterich and G. Xu, Effect of initial conditions and loading path on earthquake nucleation. *Submitted to J. Geophys. Res.*, 2009a.

[42] Fang, Z., J. H. Dieterich, K. B. Richards-Dinger and G. Xu, Earthquake nucleation on faults with non-constant normal stress. *Submitted to J. Geophys. Res.*, 2009b.

[43] Frye, K. M., and C. Marone, The effect of humidity on granular friction at room temperature, *J. Geophys. Res*., *107*, doi:10.1029/2001JB000654, 2002.

[44] Harris, R. A., R. J. Archuleta, and S. M. Day, Fault steps and the dynamic rupture process: 2-D numerical simulations of a spontaneously propagating shear fracture, *Geophys. Res. Lett.*, *18*, 893-896, 1991.

[45] Harris, R. A., and S. M. Day, Dynamics of fault interaction: Parallel strike-slip faults, *J. Geophys. Res.*, *98*, 4461-4472, 1993.

[46] Harris, R. A., J. F. Dolan, R. Hartleb, and S. M. Day, The 1999 Izmit, Turkey, earthquake: A 3D dynamic stress transfer model of intra-earthquake triggering, *Bull. Seismol. Soc. Am.*, *92*, 245-255, 2002.

[47] Heslot, F., T. Baumberger, B. Perrin, B. Caroli, and C. Caroli, Creep, stick-slip, and dry friction dynamics: experiments and a heuristic model, *Phys. Rev. E*, *49*, 4973-4988, 1994.

[48] Hughes, T. J. R., *The Finite Element Method Linear Static and Dynamic Finite Element Analysis*, Prentice-Hall, Old Tappan, N. J., 1987.

[49] Ida, Y., Cohesive force across the tip of a longitudinal shear crack and Griffith's specific surface energy, *J. Geophys. Res*., *77*, 3796-3805, 1972.

[50] Kato, N., and T. Hirasawa, A numerical study on seismic coupling along subduction zones using a laboratory-derived friction law, *Phys. Earth Planet. Inter.*, *102*, 51-68, 1997.

[51] Kilgore, B. D., M. L. Blanpied and J. H. Dieterich, Velocity dependent friction of granite over a wide-range of conditions, *Geophys. Res. Lett.*, *20*, 903-906, 1993.

[52] Knuepfer, P. L. K., Implications of the characteristics of end-points of historical surface fault ruptures for the nature of fault segmentation, in *Fault Segmentation and Controls of Rupture Initiation and Termination*, edited by D. P. Schwartz and R. H. Sibson, *U.S. Geol. Surv. Open File Rep.*, *89-315*, 193-228, 1989.

[53] Lapusta, N., J. R. Rice, Y. Ben-Zion, and G. T. Zheng, Elastodynamic analysis for slow tectonic loading with spontaneous rupture episodes on faults with rate- and state-dependent friction, *J. Geophys. Res.*, *105*, 23,765-23,789, 2000.

[54] Lapusta, N., and J. R. Rice, Nucleation of rate and state frictional instability under non-uniform loading, *Eos Trans. AGU*, *83*(47), Fall Meet. Suppl., Abstract S61E-05, 2002.

[55] Lapusta, N., and J. R. Rice, Nucleation and early seismic propagation of small and large events in a crustal earthquake model, *J. Geophys. Res.*, *108*, doi:10.1029/ 2001JB000793, 2003.

[56] Li, V. C. and J. R. Rice, Pre-seismic Rupture Progression and Great Earthquake Instabilities at Plate Boundaries, *J. Geophys. Res.*, *88*, 4231-4246, 1983.

[57] Linker, M. F., and J. H. Dieterich, Effects of Variable Normal Stress on Rock Friciton: Observations and Constitutive Equations, *J. Geophys. Res.*, *97*, 4932-4940, 1992.

[58] Liu, Y., and J. R. Rice, Aseismic slip transients emerge spontaneously in three-dimensional rate and state modeling of subduction earthquake sequences, *J. Geophys. Res.*, *110*, B08307, doi:10.1029/2004JB003424, 2005.

[59] Liu, Y., and J. R. Rice, Spontaneous and triggered aseismic deformation transients in a subduction fault model, *J. Geophys. Res.*, *112*, B09404, doi:10.1029/2007 JB004930, 2007

[60] Lothe, J., Ions in anisotropic media, the interaction energy, *Philos. Mag. A*, *46*, 177–180, 1982.

[61] Lettis, W., J. Bachhuber, R. Witter, C. Brankman, C. E. Randolph, A. Barka, W. D. Page, and A. Kaya, Influence of releasing step-overs on surface fault rupture and fault segmentation: Examples from the 17 August 1999 Izmit earthquake on the North Anatolian fault, Turkey, *Bull. Seismol. Soc. Am.*, *92*, 19-42, 2002.

[62] Madariaga, R., K. B. Olsen and R. J. Archuleta, Modeling dynamic rupture in a 3D earthquake fault model, *Bull. Seismol. Soc. Am.*, *88*, 1182-1197, 1998.

[63] Magistrale, H., and S. M. Day, 3D simulations of multi-segment thrust fault rupture, *Geophys. Res. Lett.*, *26*, 2093-2096, 1999.

[64] Marone, C., Laboratory-derived friction laws and their application to seismic faulting, *Annu. Rev. Earth Planet. Sci.*, *26*, 643-646, 1998.

[65] Nielsen, S. B., Free surface effects on the propagation of dynamic rupture, *Geophys. Res. Lett.*, *25*, 125-128, 1998.

[66] Nielsen, S. B., and L. Knopoff, The equivalent strength of geometrical barriers to earthquakes, *J. Geophys. Res.*, *103*, 9953-9965, 1998.

[67] Oglesby, D. D., R. J. Archuleta, and S. B. Nielsen, Earthquakes on dipping faults: The effects of broken symmetry, *Science*, *280*, 1055-1059, 1998.

[68] Oglesby, D. D., and S. M. Day, The effect of fault geometry on the 1999 Chi-Chi (Taiwan) earthquake, *Geophys. Res. Lett.*, *28*, 1831-1834, 2001a.

[69] Oglesby, D. D., and S. M. Day, Fault geometry and the dynamics of the 1999 Chi-Chi (Taiwan) earthquake, *Bull. Seismol. Soc. Am.*, *91*, 1099-1111, 2001b.

[70] Oglesby, D. D., S. M. Day, Y.-G. Li, and J. E. Vidale, The 1999 Hector Mine earthquake: The dynamics of a branched fault system, *Bull. Seismol. Soc. Am.*, *93*, 2459-2476, 2003a.

[71] Oglesby, D. D., S. M. Day, and D. R. H. O'Connell, Dynamic and static interaction of two thrust faults: A case study with general implications, *J. Geophys. Res.*, *108*, doi:10.1029/2002JB002228, 2003b.

[72] Oglesby D. D., and R. J. Archuleta, The three-dimensional dynamics of a non-planar thrust fault, *Bull. Seismol. Soc. Am.*, *93*, 2222-2235, 2003.

[73] Oglesby, D. D., The dynamics of strike-slip step-overs with linking dip-slip faults, *Bull. Seismol. Soc. Am.*, *95***,** 1604-1622, 2005.

[74] Oglesby, D. D., Rupture termination and jump on parallel offset faults, *Bull. Seismol. Soc. Am.*, *98***,** 440-447, 2008.

[75] Ohnaka, M., Y. Kuwahara, and K. Yamamoto, Constitutive relations between dynamic physical parameters near a tip of the propagating slip zone during stick-slip shear failure, *Tectonophysics*, *144*, 109-125, 1987.

[76] Ohnaka, M. and T. Yamashita, A cohesive zone model for dynamic shear faulting based on experimentally inferred constitutive relation and strong motion source parameters. *J. Geophys. Res.*, *94*, 4089-4104, 1989.

[77] Ohnaka, M. and Y. Kuwahara, Characteristic features of local breakdown near a crack-tip in the transition zone from nucleation to unstable rupture during stick-slip shear failure, *Tectonophysics*, *175*, 197-220, 1990.

[78] Ohnaka, M., Nonuniformity of the constitutive law parameters for shear rupture and quasistatic nucleation to dynamic rupture: A physical model of earthquake generation processes, *Proc. Natl. Acad. Sci. USA*, *93*, 3795-3802, 1996.

[79] Ohnaka, M., and L. F. Shen, Scaling of the shear rupture process from nucleation to dynamic propagation: Implications of geometric irregularity of the rupturing surfaces, *J. Geophys. Res.*, *104*, 817-844, 1999.

[80] Okubo, P. G. and J. H. Dieterich, Effects of physical fault properties on frictional instabilities produced on simulated faults, *J. Geophys. Res.*, *89*, 5,817-5,827, 1984.

[81] Okubo, P. G., Dynamic rupture modeling with laboratory-derived constitutive relations, *J. Geophys. Res*., *94*, 12,321-12,335, 1989.

[82] Palmer, A. C., and J. R. Rice, The growth of slip surfaces in the progressive failure of over-consolidated clay slopes, *Proc. R. Soc. Lond.*, *A332*, 537, 1973.

[83] Peacock, S. M., and K. Wang, Seismic consequences of warm versus cool subduction metamorphism: Examples from southwest and northeast Japan, *Science*, *286*, 937-939, 1999.

[84] Poliakov, A. N. B., R. Dmowska, and J. R. Rice, Dynamic shear rupture interactions with fault bends and off-axis secondary faulting. *J. Geophys. Res.*, *107*, 2295, doi:10.1029/2001JB000572, 2002.

[85] Rice, J. R., and A. L. Ruina, Stability of steady frictional slipping, *J. Appl. Mech.*, *50*, 343-349, 1983.

[86] Rice, J. R., Spatio-temporal complexity of slip on a fault, *J. Geophys. Res.*, *98*, 9885-9907, 1993

[87] Rice, J. R., N. Lapusta and K. Ranjith, Rate- and state- dependent friction and the stability of sliding between elastically deformable solids, *J. Mech. Phys. Solids*, *49*, 1865-1898, 2001.

[88] Rubin, A. M., and Ampuero, J. P., Earthquake nucleation on (aging) rate- and state-faults, *J. Geophys. Res.*, *110*, B11312. doi: 10.1029/2005JB003686, 2005.

[89] Ruina, A. L., Slip instability and state variable friction laws, *J. Geophys. Res.*, *88*, 10,359-10,370, 1983.

[90] Scholz, C. H., Earthquakes and friction laws, *Nature*, *391*, 37-42. 1998.

[91] Shi, B., A. Anooshehpoor, and Y. Zeng, Dynamics of thrust faulting: 2D lattice model, *Bull. Seismol. Soc. Am.*, *88*, 1484-1494, 1998.

[92] Shibazaki, B., Nucleation of large earthquakes determined by the seismic-aseismic boundary: agreement between models and observations, *Phys. Earth Planet. Int.*, *134*, 129-138, 2002.

[93] Shibazaki, B., and Y. Iio, On the physical mechanism of silent slip events along the deeper part of the seismogenic zone, *Geophys. Res. Lett.*, *30*, doi:10.1029/2003 GL017047, 2003.

[94] Sieh, K., et al., Near-field investigations of the Landers earthquake sequence, April to July 1992, *Science*, *260*, 171– 176, 1993.

[95] Stesky, R. M., Mechanisms of high temperature frictional sliding in Westely granite, *Can. J. Earth Sci.*, *15*, 361-375, 1977.

[96] Stuart, W. D., Strain softening prior to two-dimensional strike-slip earthquakes, *J. Geophys. Res.*, *84*, 1063-1070, 1979.

[97] Stuart, W. D., and G. M. Mavko, Earthquake instability on a strikeslip fault, *J. Geophys. Res.*, *84*, 2153-2160, 1979.

[98] Stuart, W. D., R. J. Archuleta, and A. G. Lindh, Forecast model for moderate earthquakes near Parkfield, California, *J. Geophys. Res.*, *90*, 592-604, 1985.

[99] Stuart, W. D., Forecast model for great earthquakes at the Nankai Trough subduction zone, *Pure Appl. Geophys.*, *126*, 619-641, 1988.

[100] Stuart, W. D., and T. E. Tullis, Fault model for preseismic deformation at Parkfield, California, *J. Geophys. Res.*, *100*, 24,079-24,099, 1995.

[101] Tse, S. T. and J. R. Rice, Crustal earthquake instability in relation to the depth variation of frictional slip properties, *J. Geophys. Res.*, *91*, 9452-9472, 1986.

[102] Tullis, T. E. and J. D. Weeks, Constitutive behavior and stability of frictional sliding of granite, *Pure Appl. Geophys.*, *124*, 383-414, 1986.

[103] Tullis, T. E., Rock friction constitutive behavior from laboratory experiments and its implications for an earthquake prediction field monitoring program, *Pure Appl. Geophys.*, *126*, 555-588, 1988.

[104] Uenishi, K., and J. R. Rice, Universal nucleation length for slip weakening rupture instability under nonuniform fault loading, *J. Geophys. Res.*, *108*, doi:10.1029 /2001JB001681, 2003.

[105] Wang, W. and C. H. Scholz, Micro-mechanics of the velocity and normal stress dependence of rock friction, *Pure Appl. Geophys*, *143*, 303-315, 1994.

[106] Wesnousky, S. G., Seismological and structural evolution of strike-slip faults, *Nature*, *335*, 340-343, 1988.

[107] Xu, G., and M. Ortiz, A variational boundary integral method for the analysis of 3D cracks of arbitrary geometry modeling as continuous distributions of dislocation loops, *Int. J. Numer. Methods Eng.*, *36*, 3675-3701, 1993.

[108] Xu, G., A. S. Argon, and M. Ortiz, Nucleation of dislocations from crack tips under mixed modes of loading: Implications for brittle against ductile behavior of crystals, *Philos. Mag. A*, *72*, 415-451, 1995.

[109] Xu, G., A variational boundary integral method for the analysis of 3D cracks of arbitrary geometry in anisotropic elastic solids, *J. Appl. Mech.*, *67*, 403– 408, 2000.

[110] Xu, G., and C. Zhang, Analysis of dislocation nucleation from a crystal surface based on the Peirls-Nabarro dislocation model, *J. Mech. Phys. Solids*, *51*, 1371-1394, 2003.

[111] Zachariasen, J., and K. Sieh, The transfer between two echelon strike slip faults: A case study from the 1992 Landers earthquake, Southern California, *J. Geophys. Res.*, *100*, 15,281-15,301, 1995.

[112] Zampier, D., M. Massironi, R. Sedea, and V. Sparacino. Strike-slip contractional stepovers in the Southern Alps, *Eclogae Geol. Helv., 96*, 115-123, 2003.

[113] Zhang, C., D. D. Oglesby, and G. Xu, Earthquake nucleation on dip-slip faults, *J. Geophys. Res.*, 109, B11302, doi: 10.1029/2003JB002894, 2004.

[114] Zhang, C., D. D. Oglesby, and G. Xu, Earthquake nucleation on dip-slip faults with depth-dependent frictional properties, *J. Geophys. Res.*, *111*, B07303, doi: 10.1029/ 2004JB003575, 2006.

[115] Zoback, M., R. C. Jachens, and J. A. Olson. Abrupt along-strike change in tectonic style: San Andreas Fault zone, San Francisco Peninsula, *J. Geophys. Res.*, *104*, 10,719-10,742, 1999.